HHS Public Access

Author manuscript

Supercond Sci Technol. Author manuscript; available in PMC 2020 August 28.

Published in final edited form as:

Supercond Sci Technol. 2014 ; 27(10): . doi:10.1088/0953-2048/27/10/103001.

Progresses and challenges in the development of high-field solenoidal magnets based on RE123 coated conductors

Carmine Senatore[1], **Matteo Alessandrini**[2], **Andrea Lucarelli**[2], **Riccardo Tediosi**[2], **Davide Uglietti**[3], **Yukikazu Iwasa**[4]

[1]Département de Physique de la Matière Condensée (DPMC) and Département de Physique Appliquée (GAP), University of Geneva, Geneva CH-1211, Switzerland [2]Bruker Biospin AG, Fallanden, Switzerland [3]EPFL-CRPP, Fusion Technology, 5232 Villigen-PSI, Switzerland [4]Francis Bitter Magnet Laboratory, Massachusetts Institute of Technology, Cambridge, MA 02139, USA

Abstract

Recent progresses in the second generation $REBa_2Cu_3O_{7-x}$ (RE123) coated conductor (CC) have paved a way for the development of superconducting solenoids capable of generating fields well above 23.5 T, i.e. the lim it of NbTi-N b_3Sn-based magnets. However, the RE123 magnet still poses several fundamental and engineering challenges. In this work we review the state-of- the-art of conductor and magnet technologies. The goal is to illustrate a close synergetic relationship between evolution of high-field magnets and advancement in superconductor technology. The paper is organized in three parts: (1) the basics of RE123 CC fabrication technique, including latest developments to improve conductor performance and production throughput; (2) critical issues and innovative design concepts for the RE123-based magnet; and (3) an overview of noteworthy ongoing magnet projects.

Keywords

REBCO coated conductors; superconducting magnets; magnet technology

1. Introduction

Discovery in 1986 of high-temperature superconductivity (HTS) changed the attitude toward superconductivity of many people, inside science and engineering and even outside. Because for the very first time the remarkable potentials of superconductivity, much touted for so long, appeared much closer to the real world, at least as real as readily accessible liquid nitrogen compared with remote and esoteric world of liquid helium. Although the 77 K barrier was first broken by $YBa_2Cu_3O_{7-x}$ (YBCO) in the *bulk* form [1], YBCO was quickly followed by $(BiPb)_2Sr_2Ca_{n-1}Cu_nO_{2n+4}$, known BSCCO that comes in two varieties, Bi2212 ($n = 2$) and Bi2223 ($n = 3$) [2]. From the get-go, BSCCO fabricated in *wire* becam e the m ost eligible HTS for two important applications, power cables and magnets. As have been

carmine.senatore@unige.ch.

long established by NbTi and N b_3Sn magnets, the preferred conductor form is indisputably multifilamentary wire. Of the two varieties, only Bi2212 can be fabricated into multifilamentary wire. This is the vital asset of Bi2212 that has kept it relevant from the beginning. For >1 GHz (>23.5 T) NM R magnets, Bi2212, particularly with recent progress [3], is poised to become a viable alternative to the 2nd generation $REBa_2Cu_3O_{7-X}$ (RE123, RE = rare Earth) coated conductor (CC) [4]. Today, RE123 is moving towards a goal of everexpanding possibilities and opportunities in a three-legged race with its most important partner, the magnet. This paper covers challenges to and recent progress in the RE123 and high-field superconducting magnets. The paper first discusses RE123 issues, including preparation techniques, strategies to reduce critical-current anisotropy, and stress effects on critical current. Most of the second half is devoted on magnet technology, specifically on winding techniques, quench protection, and field quality. The paper ends with an overview of six high-field magnets that rely partly or wholly on RE123 coils.

2. RE123 CCs for magnet applications

In the last ten years the RE123 CCs have attracted m ost of the attention in the applied superconductivity research. The reasons for this excitement are their high current densities in high magnetic fields, their outstanding mechanical properties (with Hastelloy or stainless steel as substrate) and, above all, a prospect of economically viable conductor prices.

The development of practical superconductors based on RE123 has revolved around the complexity of achieving high critical current densities in polycrystalline materials. The problem lies in the build up of charge inhomogeneities and strain at the grain boundaries (GBs), regions of mismatch between crystallites with misoriented crystalline axes, that act as weak links that drastically lim it the current flow [5]. Therefore, the critical current density through the RE123 GBs falls off exponentially with increasing misorientation angle θ of adjacent crystallites for θ above 5°–10° [5, 6]: it has been necessary to develop expensive and sophisticated crystallographic texture fabrication processes to eliminate all but low-angle GBs in useful conductor form. A variety of approaches have been implemented at industrial level over the years, but all rely on two common features: a biaxially textured template, consisting of a long and flexible tape-shaped metallic substrate coated with a multifunctional oxide barrier; and an epitaxial RE123 layer. In addition, for environmental protection and thermal stabilization, an Ag layer a few μm thick and a thicker Cu layer complete the conductor.

At present, the commercial development of the so-called RE123 CCs focuses on three linked issues: performance; price; and production length. On one hand manufacturers aim to improve the conductor perform ance without increasing the production costs; on the other hand they are actively pursuing new routes to simplify the wire architecture and increase the produced length and yield, with the goal to reduce the conductor price. The CC cost is mostly due to a large investment in the production infrastructure. The industry is therefore focusing on to process longer lengths of input material in each production run, increase the useful output from the equipment and thus lower the break-even price per unit length. The key ingredients to improve the performance/cost ratio are three:

- Simplify the wire architecture, the production yield being the product of the yield for each production step;
- Perform buffer and RE123 deposition on large areas, followed by a slitting operation to size the conductor to a final width;
- Increase the production line speed.

Kilometer lengths of CCs have been successfully dem onstrated and lengths of 150+ m with a minimum critical current of 350 A cm^{-1} width at 77 K and in self-field are currently available. However, the present price of ~$200 kA m (at $B = 2.5$ T, $T = 3\ 0$ K) [7] is too high for widespread marketplace applications: power device m anufacturers (transformers, motors, SMES, cables, fault-current limiters) demand a price less than $50 kA m.

In a high-field NbTi-Nb_3Sn magnet, the operating current is often limited by wire strength (hoop stress), not by critical current. Indeed, for high-field magnets in the field range 19–24 T, RE123 and Nb_3Sn costs are rather competitive. The reason is mechanical, i.e., an RE123 coil can operate at much higher electromechanical stresses than its LTS counterparts, allowing it to fully exploit available high critical current density. Moreover, in a field above ~18 T, Nb_3Sn has to be operated at 2.2 K, while RE123 at 4.2 K. Also note that the tape length required for power equipment is large compared to that for a high-field magnet: hundreds of km of tape are needed for a 1 km long power cable, whereas continuous lengths of less than 1 km and total lengths typically of ~ 1 0 km are sufficient for a high-field HTS coil.

The remaining part of the section describes the primary approaches for fabrication of a textured template and deposition of a superconducting layer and addresses the latest developments in the manufacturing process of RE123 CCs.

2.1. Preparation techniques: template texturing

In commercial CCs, the textured template is created by either deforming the metal substrate with the rolling assisted biaxially textured substrate technology (RABiTS) [8] or by texturing the buffer layers by ion beam assisted deposition (IBAD) [9]. The main features of these two technologies are briefly described below.

2.1.1. RABiTS template.—In the RABiTS approach, cube texturing is achieved in a NiW substrate through a process of rolling and recrystallization annealing [8]. Compared with pure Ni, NiW alloys exhibit reduced magnetization (Curie temperatures of 335 K for Ni5 at.%W and 630 K for Ni) and higher mechanical strength (yield strengths of ~ 150 M Pa at room temperature for Ni5 at.%W and ~ 7 0 M P a for Ni).

Ni5 at.%W substrates are industrially prepared in the form of a flexible strip, typically 75 μm thick and more than 1 km long. The x-ray full-width half-maximum (FWHM) of the diffraction peak referring to the in-plane texture of the substrate along the entire production length is $\Delta\varphi \sim 6–7°$ [10]. The out-of-plane ($\Delta\chi$) FW HM values average approximately 7° [10]. After plasm a cleaning to reduce surface roughness, epitaxial buffer layers m ust be deposited to provide a lattice- matched surface ready for the growth of an HTS layer.

The first layer is typically Y_2O_3 (AMSC [10],) or CeO_2 (Sumitomo [11]). This seed layer achieves an out-of-plane texture that is sharper than the NiW substrate. This is a key step in the production of the RABiTS template. The second yttrium-stabilized zirconia (YSZ) layer behaves as a blocking layer for the inter-diffusion of substrate atoms. Top CeO_2 is then prepared to compensate the lattice mismatch between the superconductor and the YSZ layer. The enhanced texture of the seed layer with respect to the substrate propagates throughout the subsequent YSZ and CeO_2 buffer layers. This template results in an improvement of ~3° in $\Delta\chi$ and ~1° in $\Delta\varphi$ [12] compared with the NiW tape. All buffer layers are grown by RF-sputtering. The layer thickness varies among manufacturers, but it is typically of the order of 100 nm.

Further developments of the RABiTS technology are oriented towards substrates characterized by a reduced ferromagnetic behavior, in order to lower the hysteretic losses especially for power applications. To this end, higher W -content NiW substrates with the qualified cube texture are being developed [13], but also new preparation approaches for composite substrates are reported [14]. The concept of a com posite substrate is to have a thin biaxially textured Ni5at. %W layer on a non-magnetic Ni9at.% W base substrate. Although the biaxially textured layer in this clad-type substrate is ferromagnetic, the overall magnetization is reduced.

2.1.2. IBAD template.—The IBAD technique generates a preferred texture in the buffer layer, hence it does not require a textured substrate. Polycrystalline Hastelloy or stainless steel tapes (typical 50–100 μm thick) are submitted to an electropolishing process. This process reduces surface roughness from ~ 50 nm to less than 2 nm [15]. On the polished substrate surface an Al_2O_3 diffusion-barrier and an Y_2O_3 seed layers are deposited by sputtering technique. The Al_2O_3 and Y_2O_3 layers are 100–200 nm and 10–20 nm thick, respectively [16]. A biaxially textured MgO layer is then grown on the Y_2O_3 layer with the IBAD. This technique deposits MgO in a standard PLD geometry, using a RF plasm a source that assists ion beam. The assisting ion is typically Ar^+ with beam energy of ~ 1 keV and an irradiating angle between 45° and 55° from the substrate normal.

Two mechanisms have been proposed to explain how ion beams affect the crystallographic orientation of growing films. The variation of growth rate with crystal orientation is associated with the existence of crystallographic directions along which ions easily penetrate into the crystal. Consequently, grains having these channeling directions aligned parallel with the ion beam have a higher growth rate than non- aligned grains. The second mechanism is related to the recrystallization on the substrate. The aligned grains are less damaged than non-aligned grain by the ions. During the thermal spike associated with ion bombardment, the aligned grains can grow into their more damaged surroundings, thereby reorienting the more damaged material [17]. Typically an appropriate texture is achieved for a very thin layer (<10 nm), though a homoepitaxial layer of MgO (~ 50nm) [15] is often added. The typical in-plane texture $\Delta\varphi$ in the MgO layer is <10° [16].

The next process may vary among manufacturers. At Fujikura, a 500 nm thick CeO_2 layer is deposited on MgO and a sharp in-plane texture $\Delta\varphi = 4°$ is obtained [18]. SuperPower,

SuNAM and SuperOx grow a LaM nO_3 layer (20–30 nm) by sputtering atop the homoepitaxial MgO [15, 19, 20].

A variant of the IBAD process, the alternating beam assisted deposition (ABAD), has been developed by Bruker [21]. In this approach, the substrate, first exposed to a molecular flow provided by a sputter source, acquires a few nanometer-thick layer of YSZ. In the following step this layer undergoes an ion etching with an Ar^+ ion beam. After several tens of deposition-etching cycles, a sufficiently high in-plane texture (with FW HM = 8–9°) is achieved in the YSZ layer. A high rate pulsed laser deposition (HR-PLD) is then used for growing a ~0.1 *μm* thick CeO_2 cap layer.

The American manufacturer STI has focused on the development of a simplified IBAD architecture where the unpolished Hastelloy substrates are planarized by a solution deposition process (SDP) [22], eliminating the need for an electropolishing step. The idea is to coat the unpolished substrate with a liquid solution: the liquid surface tension planarizes the free surface, resulting in thicker layers over valleys and thinner layers over peaks, overall, a smoother surface than that with the underlying substrate. Specifically, several coatings of Y_2 O_3 and Y_2 O_3–Al_2O_3 mixtures are used to planarize the substrate, leading to a surface roughness of less than ~ 2 n m. SDP has thus the advantage of replacing three steps: electropolishing; barrier; and nucleation layer deposition. The material deposited by SDP is then used as a bed layer for the IBAD and homoepitaxial MgO. In the STI template, HTS is deposited on the MgO layer without the need for additional epitaxial buffers, such as LaM nO_3 or CeO_2.

It should be stressed that for power applications both NiW and Hastelloy/Steel substrates can be used, while for high-field magnets the substrate mechanical strength of Hastelloy trumps that of NiW. Indeed, this superior m echanical strength makes the Hastelloy-substrate RE123 CC a preferred option to all other HTS for high-field (>20 T) magnets.

2.2. Preparation techniques: RE123 layer deposition

In commercial CCs multiple techniques for depositing epitaxial RE123 are presently being adopted, with a goal of achieving a low-cost flexible process that is also easily scalable to mass industrial production. Table 1 lists key parameters of the CCs among manufacturers. The RE123 layer can be deposited either by chemical routes, such as metal organic deposition (MOD) [23] and metal organic chemical vapor deposition (MOCVD) [24], or by physical routes, such as pulsed laser deposition (PLD) [11, 16, 25, 26] and reactive co-evaporation (RCE) [15, 22]. MOD and RCE are *ex situ* processes incorporating two steps: deposition of the precursors and subsequent conversion of the precursors into RE123. On the other hand, deposition and formation occur simultaneously during *in situ* processes such as PLD and MOCVD.

The basic principles defining these alternative approaches currently used at industrial level are summarized in the following subsections.

2.2.1. Metal organic deposition (MOD).—

In the MOD process a solution of fluorine-based organic precursors bearing the stoichiometric proportions of cations for forming

RE123 is deposited on the substrate by dip-coating [23]. The technology developed at AMSC for commercial HTS wires is based on this approach. In MOD the control of the coating thickness is achieved by fine-tuning the solution concentration and viscosity. The coating is then dried and decomposed at temperatures below 600 °C to remove carboncontaining materials, leaving a mixture of yttrium–barium–oxyfluoride, Y_2O_3, and copper oxides. The decomposition temperature profile is carefully controlled to prevent cracking of the film, which is ~20 μm thick as it enters the decomposition process. This film is subsequently reacted at temperatures in the range 700–800 °C in an O_2–H_2O environment to form RE123. A silver passivation layer, several micrometers thick, is then deposited, followed by an oxygen anneal to optimize the RE123 performance. With a single coating step it is possible to achieve 0.8 μm effective RE123 thickness (corresponding to approximately 1 μm actual thickness including porosity and secondary phases), but the coating and decomposition processes can be repeated multiple times to achieve thicker layers and thus increase the overall critical current. Recently, ink jet printing has appeared as an interesting alternative to the dip-coating deposition of the precursors, although only demonstrated at laboratory scale for the time being [27, 28]. In this approach thermal or piezoelectric print heads dispense small droplets of consistent volume of the precursor solution on the substrate. This allows a better control of film thickness, precise positioning (including patterning, if necessary), solution waste minimization, and reproducibility. Presently, Oxolutia and Deutsche Nanoschicht are working to scale it up to the industrial level.

2.2.2. Metal organic chemical vapor deposition (MOCVD).—MOCVD is a proven process for large-scale manufacturing of several materials and it was successfully adapted to RE123 by SuperPower [24]. It is a multistep process. Organic precursors are used for Y (or other rare Earth materials), Ba, and Cu. In the first step, the liquid precursors are vaporized at a constant temperature. The vaporized precursors then flow in a carrier gas of argon and oxygen and are injected onto a hot substrate. RE123 films, typically ~1 μm thick, are deposited within a temperature regime of 700–800 °C in partial oxygen pressure. The deposition temperature is optimized to achieve a dense film structure as well as to minimize coarsening of particulates. If the film thickness is increased, a dead layer formed by secondary phases, pores, and misaligned grains nucleates grows on the RE123 surface. However, this problem can be overcome with a multi-pass technique, i.e. depositing multiple layers of RE123 one atop each other in individual passes.

2.2.3. Pulsed laser deposition (PLD).—The PLD process, widely used in the development of the CC technology, has been recently optimized by various manufacturers (Bruker, Fujikura, SuperOx and Sumitomo) and scaled up to production lengths [11, 16, 20, 21, 26]. A pulsed ultraviolet laser, typically an excimer laser from KrF or XeCl, irradiated a sintered target with the desired composition to form a superconducting layer. The ablation of RE123 bulk material requires a laser fluence of 10–30 mJ mm^{-2} [29, 30]: the target material is vaporized in a plasma plume and deposited on the substrate.

It is known that to insure good film stoichiometry the film thickness per one deposition pulse should not exceed 0.1 nm. Moreover, the pulse repetition rate must be kept below ~50 Hz to

prevent deterioration of the critical current density. Bruker and Fujikura adopted a technique based on scanning the laser beam over a large-area target [18, 20]. The laser plume produced in the course of such scans causes a film deposition in random sequence of small areas over a largearea substrate, which is also smoothly moved during the film deposition. The target and substrate scans are performed independently in time, and, therefore, insure a homogeneous film thickness and stoichiometry. Under such conditions, the repetition rate of laser pulses can be increased by a factor of 10^3 while the local repetition rate of the deposition pulses is kept at the low level of <20 Hz. The film thickness obtained by one pass is generally about 0.3–0.5 μm, and thus multiple layers have to be deposited in order to acquire a high critical current.

2.2.4. Reactive co-evaporation (RCE).—In the RCE process Y (or Gd), Ba, and Cu are individually heated to evaporate and deposit them on the substrate. Atomic absorption spectroscopy is used to measure the vapor density close to the sources and fine-tune the heater power, in order to adjust the film composition. Two manufacturers adopted this approach, but with some differences.

At SuNAM the film is deposited in a single step. Then, the as-deposited amorphous film is passed through a tube furnace at 860 °C with two different oxygen pressures (10^{-2} mTorr and 150 mTorr) and during a rapid oxidation process the amorphous film is converted in Gd123 [31, 32]. At STI the superconducting layer is formed in a cyclic process of deposition and reaction [22]. The sample alternates on a fast time scale between a low-pressure region, where it receives a deposit from the sources, and a high-pressure region (p_{O2} ≈20 mTorr), where it is oxidized, forming a superconducting layer. Co-evaporated materials are deposited on substrates wound on a rotating drum heated at 700 °C–800 °C. As reported [22], the drum rotation is adjusted to obtain a ratio of coating time to oxidation time of 1:9. With a 5 Hz rotation speed and a 6 nm s^{-1} evaporation rate, approximately 0.12 nm is deposited per pass, giving an average deposition rate of 0.6 nm s^{-1}. In this way 1 μm thick film can be deposited in 30 min.

As a closing remark to this section, it should be stressed that selecting a suitable deposition strategy for magnet applications is a very complex decision because technical aspects need to be inevitably balanced with commercial aspects and reframed within the existing market prospective. It is in fact not easy for tape manufacturers to cover the broad spectrum of specifications defined by the various industries interested in CCs. On one hand, the electric utility sector, representing a huge potential market for HTS conductors, has less stringent requirements in terms of single-piece length but demands both large current-carrying capacities and production capabilities. On the other hand, coil manufacturers are interested in longer, continuous lengths and enhanced mechanical properties for the market potentials much smaller than those for the electric utility sector. Achieving long, defect-free wire lengths is a true challenge that forces manufacturers to simultaneously increase the batch length and improve the process yield (defect-free length/km of processed conductor). High yield of course tremendously impacts product price especially in a small market. If production volume could be increased and the process throughput simultaneously enhanced, the rate at which longer lengths could be available would be also higher without necessarily working on the reduction of the number of defects per unit length. In this equation, as

presented earlier in the section, throughput and batch size are the only parameters directly controllable by the wire manufacturers. Processes that allow depositing the ceramic superconductor at higher rates and over larger processing areas may, in the long run, facilitate efficient production of long lengths. A solid organic growth of the HTS conductor demands will in any case remain the main driver favouring the production of long lengths.

2.3. Strategies to reduce the anisotropy of critical current density (J_c)

Field-dependent J_c of RE123 tape depends importantly on θ, the angle between field direction and the RE123 crystallographic orientation, here, θ=0° and θ=90° defined, respectively, when field is parallel to the ab-plane (tape surface) and the *c*-axis (normal to tape surface). The anisotropy makes J_c maximum at θ=0° and minimum near θ=90° and the ratio of the current densities in the two orientations tends to increase with increasing magnetic field. By itself, the conductor anisotropy is not detrimental but it introduces an extra layer of complexity in the magnet design process. In a magnet, the conductor is exposed to a magnetic field whose angle depends on its position in the winding. This implies that the loadline at each point of an HTS coil virtually intercepts a different $J_c(B)$ curve. A careful adaptation of the magnet design process to the specific anisotropic conductor characteristic is necessary in order to determine criticalities and safety margins of each design.

In order to minimize the effect of anisotropy and limit the complexity of the design process, artificial pinning centers are being implemented. Over the last few years, extensive research has been conducted on $BaZrO_3$ (BZO) additions. Enhanced flux pinning has been obtained by BZO-incorporated RE123 thin films made by PLD [33], MOCVD [34] and MOD [35]. Depending on deposition technique, the morphology and size of the precipitates and thus the effects on the pinning properties are different.

PLD and MOCVD lead to the formation of anisotropic nanorods (~5 nm in diameter, >100 nm in length) that grow along the *c*-axis [36, 37]. The intrinsic weak pinning in the magnetic field parallel to the *c*-axis is thus reinforced by the interaction between nanorods and vortices. On the other hand, MOD produces distributed BZO-nanodots (10–50 nm in size), resulting in a more isotropic pinning landscape [38]. In both cases, the enhanced pinning has been correlated to the nanostrain emerging from the interfaces between the BZO inclusions and the RE123 matrix [38]. It is possible to introduce BZO inclusions also in RE123 films grown by RCE. However, the required control of the precipitates' shape and dimensions and thus the positive effects on J_c are not yet achieved with this deposition technique. In a recent work on the SuNAM tapes [39] it was shown that RCE leads to the formation of uniformly dispersed Gd_2O_3 particles in the Gd123 layer. The refinement of these Gd_2O_3 particles seems to be a promising alternative to BZO for enhancing pinning in CCs processed by RCE [32].

In figure 1 the angular dependences of I_c at T=77 K, B=1 T are compared for RE123 tapes fabricated by MOCVD with and without BZO inclusions [40]. BZO leads to a twofold enhancement of I_c in the orientation of B perpendicular to the tape surface (at angles around 180° in figure1). However, at temperatures below ~40 K BZO nanorods do not lead to any *c*-

axis peak, even when the critical current values are higher compared with those of the undoped samples (figure 2) [41].

The impact of anisotropy on magnet design is very application-specific and depends from several factors like the geometry of the HTS coil itself (winding thickness, coil length, inner diameter), the presence, design and position of external magnetic sources (outserts) and the coil operating conditions (in particular temperature and ramping/cooling strategies). Specifically, for high-field magnets, the most critical regions are usually located at the extremities of the HTS coil where the value of the field perpendicular to the crystallographic ab-plane is highest due to the combined effect of the HTS self-field and the outsert field [42].

Although not based on conductor technology, some strategies have been proposed to minimize the detrimental effects of the anisotropy. One of these, the multi-width (MW) winding technique [43], is applicable to a magnet comprising an assembly of double-pancake coils. It consists in grading the conductor width of the double pancake coils, assigning the narrowest to magnet regions near the magnet midplane and the widest to those at and near the magnet ends where, as stated above, the tape performance degradation by perpendicular field components is greatest.

Generally speaking, isotropic wires are desirable mainly because not only the wire performance is independent of field direction but also the design and magnet construction processes can rely on many years of experience with LTS conductors for many magnets, e.g., high-field laboratory, NMR and MRI magnets. For this reason, the concept of round wires based on RE123 tapes to circumvent conductor anisotropy is also being examined within the European Project EUROTAPES consortium [44]: a proposed idea folds the CC along its longitudinal axis into a tube, with the RE123 layer placed on the neutral axis of the tape. The approach is interesting but a clear drawback will be the low bendability of such a conductor.

2.4. Strategies to reduce hysteretic losses

For applied field above the so-called penetration field, hysteretic losses, Q_{hyst}, in a superconducting wire scale with the critical current density and with the effective size of the filaments. The multifilamentary configuration is standard for LTS, chiefly to minimize hysteretic losses. Typical values of Q_{hyst} for a field cycle ±3 T at 4.2 K are ~50 mJ cm^{-3} in NbTi wires and between 100 and 1000 mJ cm^{-3} for the various grades of Nb_3Sn wires [45]. In CCs the superconductor is of a single layer ~1 μm thick and 4–12 mm width, making its hysteretic losses strongly dependent on its effective size to the direction of a time-varying field. This size varies with the conductor orientation to the field, i.e., from ~1 μm (parallel) to 4–12 mm (perpendicular). Note that in a solenoid the radial component (i.e., perpendicular direction) of its self field increases axially away from the midplane, reaching maximum at two ends of the solenoid. Therefore, at the coil ends the hysteretic losses of a CC are much larger than in multifilamentary wires. The hysteretic losses depend on the effective filament size and thus in CCs AC losses are expected to be 2–3 order of magnitudes higher than those in LTS wires (as much as 4–12 mm wide in CCs against ~1 μm filament size in NbTi wires) and at least one order of magnitude higher losses than in Bi2212 and

Bi2223 tapes, though their effective sizes are <1 mm, are, unlike LTS filaments, magnetically well coupled. In the perpendicular orientation Q_{hyst} (4.2 K) well above 10^4 mJ cm^{-3} have been reported for CCs on the IBAD Hastelloy substrate [46]. In the RABiTS approach, additional hysteretic losses arise from the ferromagnetic substrate and this is making AMSC to switch from Ni5 at.%W to a non-magnetic Ni9 at.%W substrate [13].

Special conductor designs are needed to minimize the conductor's susceptibility to large AC losses on perpendicular field. In particular, the subdivision of the RE123 layer into parallel filaments along the tape axis has been explored at laboratory scale either using subtractive processes, e.g., chemical etching [47], ion implantation [48] and laser ablation [49] or by direct printing of multifilamentary structures through ink jet deposition [50]. The typical width of the RE123 strips is in the order of 100 μm, with an inter-stripe separation of ~100 nm. In some cases striation is achieved by completely removing material, in others by degrading the superconducting properties of the inter-stripe region [48, 51]. Also the silver cap layer and copper stabilizer on the top of the superconductor have to be striated to prevent from coupled filaments [47]. However, it is not a straightforward task to develop an economically viable process to achieve such structures over industrial lengths. Even these techniques of slitting the superconductor into many parallel narrow strips do not address to minimize another source of AC losses: coupling losses between filaments.

2.5. Effects of mechanical loads on I_c

2.5.1. Reversible effects of strain.—

Due to the intrinsic brittleness of the RE123 layer, electromagnetic strain during operation may degrade irreversibly the critical current of a CC. The irreversible limits under axial and transverse mechanical loads are mainly determined by the conductor architecture and will be treated in sections 2.5.2 and 2.5.3. Below the irreversible strain limit beyond which the superconducting layer is damaged, strain affects I_c reversibly, i.e., I_c returns to its initial value when the strain is released.

As recently shown by Sunwong *et al* [52], the normalized I_c for CCs follows an almost parabolic dependence as a function of strain, independent of angle and magnetic field up to B/B_{c2} =0.4 (figure 3). This behavior is dissimilar to that observed in Nb_3Sn wires, where the effects of applied strain on the critical current become more pronounced when B/B_{c2} increases [53]. The difference is attributed to the stronger strain dependence of the superconducting parameters B_{c2} and T_c in Nb_3Sn compared with that in the biaxially textured RE123 layer.

The single crystal data on Y123 show that the dependence of T_c on applied pressure is highly anisotropic within the ab-plane of the crystal lattice [54]. T_c increases with pressure applied along the *b*-axis, dT_c/dp_b being ~2 K GPa^{-1}, whereas it decreases with the same rate when pressure is applied along the *a*-axis. In a CC, RE123 grains are generally oriented either with the *a*-axis or with the *b*-axis along the conductor length and the two orientations are equally distributed. Therefore strain applied along the conductor length is locally oriented either along the *a*-axis or along the *b*-axis of the RE123 grains. This implies that the average superconducting properties of the RE123 layer do not depend on strain, but how far the values of T_c and B_{c2} for the grains are dispersed with respect to the average value does depend on strain. The maximum in the I_c versus strain curve corresponds to an optimum

strain state where the overall T_c and B_{c2} distributions are lowest. On the other hand, critical current becomes almost insensitive to strain when CCs are prepared with *a*- and *b*- axis of the RE123 film rotated by 45° from the longitudinal direction (figure 4) [55, 56]. The reversible effects of strain on I_c are also influenced by other parameters:

- Strain sensitivity depends on the composition of the superconducting layer. In particular, Gd123 CCs exhibit a lower strain sensitivity of I_c compared with Y123 conductors [57];
- Mismatch in thermal contraction among the different components of a CC as it is cooled generates a thermal residual strain in the RE123 film, which depends on the conductor architecture;
- Peak strain value may change with applied field [58, 59]. These changes do not depend on microscopic mechanisms related to superconductivity, but are attributed to the field and strain dependence of the normal properties of the GBs [52].

2.5.2. Irreversible limit under axial loads: influence of the conductor design.

—Due to the large fractional section area of metallic substrates, mechanical strength is a big asset of RE123 CC compared with BSCCO tape and wire. With stainless steel (SS) or Hastelloy substrate the critical axial stress (95%-retention I_c) can reach, depending on the Cu fractional area, 700 MPa. However, the strength gap between RE123 and BSCCO conductors is reducing. It has been recently shown that the maximum tensile stress of Bi2223 tapes can be improved up to 430 MPa by a new lamination technique [60]. On the other hand, the increase in current density of Bi2212 wires [3] leaves room for the introduction of mechanical reinforcement in the winding, without sacrificing the overall current density.

The composite architecture of the main industrial CCs is summarized in table 2. Some manufacturers may apply a lamination technique to elongate the reversible strain, or just to add the required electrical stabilization. I_c degradation of 5% is often measured at 0.3–0.5% strain, depending on the deposition technology and on the substrate. The highest strain limits may be achieved for tape laminated with a material of large thermal contraction. After the RE123 film is deposited, the substrate and the electrical stabilizer (or the laminated support), because of their large coefficients of thermal expansion (CTE), pre-compresses the film. Different precompressions are obtained by a combination of different materials of substrate, stabilizer and laminated support [61]. Interestingly, Hastelloy substrate contracts only slightly more than RE123 film, resulting in a negligible precompression induced the film.

In 2005 Shin *et al* [62], investigated the effect of stabilizer layer on critical current for a PLD-Y123 CC deposited onto a 50 μm thick NiW substrate. In particular, their results showed that a 70 μm thick laminated SS tape significantly increases the irreversible tensile strain, because SS contracts more than NiW, inducing a large precompression in the superconductor layer. Apparently, the resultant precompression is large enough to be beneficial but not too large to damage the superconducting layer. The method can thus be used to enhance the irreversible limit of the CC. Moreover, the irreversible strain of the non-

laminated tape was 0.21%, while it was 0.44% for laminated tape. Sumitomo researchers have adopted a similar approach to precompress their DI-BSCCO tape by laminating the bare conductor with pretensioned tape [63].

More recently, the same authors [64] have compared the effects of a brass lamination placed on top of different commercial RE123 tapes. Results showed that brass can enhance the irreversible strain limit by more than 0.2%, but clearly at the expense of engineering critical current density J_{eng}. In general, these data seem to evince that any lamination carried out with materials weaker than the substrate will degrade the maximum critical hoop stress at any given J_{eng} (referring to a solenoidal coil), even if the laminated material has a high CTE.

Regarding the electroplated copper, this stabilizer will be in annealing state as long as the temperature does not fall below 350–400 °C after the deposition process. Only below these temperatures Cu will start to precompress the RE123 film. And even if the CTE of copper is very high, its influence is smaller than SS substrate (or Hastelloy), because the Young modulus of SS or Hastelloy is almost double that of copper.

Although the substrate withstands quite well high deposition temperature, the temperature dependences of its mechanical properties (Young modulus, yield stress, CTE) should be taken into account. Moreover, a SS substrate contracts more than Hastelloy (e.g. 35% higher contraction from RT to 4 K). Due to this feature, tapes with SS substrates show slightly higher strain limit for the 95%-retention I_c and much higher irreversible strain limits [65]. The beneficial effect of thermal contraction is also confirmed by improvement in irreversibility strain limit in tapes measured at 4.2 K and 77 K [66]. This mechanical advantage of the SS substrate is however of little importance because of the much lower yield stress of SS—Hastelloy yields at 1 100 MPa, whereas SS starts yielding at 800 MPa. Basically, even if 95%retention I_c with SS substrate may fall at around 0.65% and with Hastelloy at 0.55%, the corresponding tape stress would be ~780 MPa for SS and ~825 MPa for Hastelloy (figure 5). For very high-field solenoidal magnets, hoop stress in the superconductor is a critical parameter, and Hastelloy is likely a better support.

In terms of J_{eng} too, the thicker SS substrate becomes less preferable to the thinner Hatelloy substrate. If SS substrate is used over Hastelloy substrate, its thickness will be greater than Hastelloy's. This is to partially compensate for the lower yielding stress of SS. Generally, the larger the ratio of substrate/stabilizer, the greater the mechanical properties and the smaller the J_{eng}.

On the other side, the SS substrate is cost-effective (it should reduce costs by 2–3 Euro/kA m at 77 K [67]), but given the today market price of the CCs, this advantage is now considered negligible. Another interesting point deserves to be mentioned: the deposition of RE123 on SS-316L has shown delamination problems in the past [68] that were attributed to a strong thermal contraction mismatch between SS and RE123. From 900 °C to room temperature SS contracts 0.4% more than RE123, while the thermal contractions of Hastelloy and RE123 are nearly the same.

Regarding enhancement of the irreversible strain limit, Cheggour *et al* [61] in 2005 reported that the stability of fracture propagation in RE123 films is strongly related to the intimate

contact among the film, the substrate, and the stabilizer. It is known that the addition of metallic layers to ceramics greatly improves the fracture toughness of these brittle phases, because metallic layer acts as crack inhibiter/ arrester.

Furthermore, the thicker the substrate the further away from the neutral axis of bending will the RE123 film find itself when wound on a coil former. If the RE123 film is kept on the radially-outer side (tension), it can be a problem for magnets requiring small bending radii (small radius coil formers). This is confirmed by the work discussed in [65] which indicates that a tape with 50 μm Hastelloy substrate can be bent on a 6 mm radius with an I_c degradation smaller than 5%, whereas a tape with 100 μm SS substrate already degrades by almost 10% when bent on a 6 mm radius, thus showing a much higher sensitivity to bending strain because of the higher intrinsic strain applied to the RE123 film.

Among available literature a few research efforts has covered also the effect of cyclic loads. Superconductors used in magnet applications are exposed to various mechanical loads during their operational lifetime. These loads are mostly due to handling during manufacturing, thermal contraction mismatches during cooling and electromagnetic forces during operation. Features such as intensity and frequency of the loads strongly depend on magnet application. Laboratory and NMR magnets are usually ramped up slowly with load frequencies of orders of magnitude lower than those found in electrical machines (motors and generators). Nevertheless, design of durable high field laboratory magnets must take into account the effect of cyclic loads on the critical current. Fatigue occurs when a material is subjected to repeated loading and unloading. CCs are manufactured with both ductile metals and brittle ceramics, and their interaction under repeated loads is cumbersome. The superconducting ceramic is extremely sensitive to the maximum applied stress, and much less to the fatigue stress ratio, i.e. the ratio between minimum and maximum stress experienced in a cycle, whereas the ductile metals could easily present fatigue strength limit in the order of 1/3 of the static one just for being exposed to large fatigue stress ratios. High stresses have higher probabilities to quickly damage the ceramic compound, whereas large fatigue stress ratio can slowly generate cracks in the metals of the composite tape. Mbaruku *et al* [69] were the first to characterize commercial CCs in cycles >100k. In particular, their work has pointed out that fatigue cracks in the RE123 layer do not occur everywhere in the sample but are localized in weak areas, starting from the sample edge and moving towards the center (likely due to the slitting process used to cut a 12 mm wide tape into three strips of 4 mm width). Their results on a standard SuperPower tape with 50 μm thick Hastelloy substrate and 20 μm thick Cu stabilizer show no degradation in I_c or n-values even after 200k cycles for an applied maximum strain of 0.367%, with a fatigue strain ratio of 0.5 at a load frequency of 0.4 Hz. Significant degradation was observed with higher maximum applied strains, or with smaller strain ratios (see figure 6). Sugano *et al* [70] reported results on samples fabricated by MOCVD on a 100 μm thick Hastelloy substrate. They found two types of fatigue mechanisms acting independently from each other: one related to failure of the Hastelloy substrate and the other related to failure of the Ag layer. More recently, Shin *et al* [71] tested IBAD/ Sm123 tapes deposited on a 80 μm thick Hastelloy substrate. Their tests have confirmed once again that the fatigue cycle limit decreases drastically at smaller strain ratios. All these tests indicate that not only a long lifetime can be expected for standard

laboratory magnets but also a maximum strain should be chosen carefully for magnets that will undergo many loading cycles.

2.5.3. Transversal stress and delamination.—The delamination problem of CCs has been known for a few years now. Indeed, RE123 CCs are made up of numbers of layers which can be modeled as adhesive lap joints, where the brittle buffer/RE123 layer is expected to bond both the substrate (on which it is deposited) and the silver layer, on top of which the copper stabilizer is usually deposited or laminated. The RE123 CC performances are degraded significantly once the brittle adhesive buffer/RE123 assembly layer detaches or breaks. Five common stresses inherent in adhesive joints can cause detachments/fractures: tensile, shear, compressive, cleavage, and peel. Tensile stress corresponds to hoop stress in a solenoidal coil. Cleavage occurs when an external force acts to open one edge of the adhesive assembly. Peel is similar to cleavage, except here an adhered part is flexible. In cleavage and peel, the detaching force acts over a small part of the adhesive bond and, therefore, the critical (cleavage and peel) strengths are much lower [72]. Recently, Maeda at Riken summarized all the mechanical properties of RE123 tape with a detailed matrix reported in table 3 [73]. The axial tension of >700 MPa refers to a 50 μm thick Hastelloy substrate tape. Also note that each stress value corresponds to a tape with electroplated copper stabilizer.

The initial work by NIST in 2007 [74] on tapes produced by AMSC suggested that the tape slitting procedure in the production process plays an important role in the delamination issue. In order to reduce the manufacturing costs of CCs, many manufacturers deposit a thin film on substrates a few cm wide. This wide tape is then slit longitudinally to produce standard tapes, e.g. 4 mm wide. This slitting deforms the substrate, which is clearly visible in micrographs of the slit tape cross-section, and also generates initial cracks in the RE123 layer that can easily propagate under a relatively small applied transverse tension. A transverse tension can in general occur on the conductor if the winding is filled with, for example, epoxy resin with unmatched thermal contractions. Without precautions, epoxy impregnation, which is a common practice in magnet technology (especially in the power sector), can easily damage the CCs. In the same paper, NIST suggested that the strength of slit CCs against delamination raised significantly by reinforcing the conductor with laminated copper strips and solder fillets at the conductor edges. They also noted that islands of relative weak material, invariably present in the conductors, result in strong I_c degradation at low transverse stress. These local microstructure weak spots may originate from production defects or during slitting procedure or both. Finally, the NIST authors argued that CCs lack a soft metallic layer that could act as an absorber to compensate for thermal mismatch during cooldown (epoxy resins contract much more than metals); on the other hand, Bi2223 tapes have a matrix of silver, a metal much more malleable than SS or Hastelloy. Indeed, delamination has never been an issue with Bi2223 coils (even if delamination tests showed strengths lower than those in CCs). The silver deforms without transferring the thermal stress to the brittle ceramic filaments of Bi2223.

In order to circumvent the delamination problems in epoxy impregnated layer wound coils, NHMFL proposed to use polyester heat-shrink tubing from Advanced Polymers [75] to decouple the tape from the epoxy. A similar problem was observed in epoxy-impregnated

double pancake coils by Takematsu *et al* [76]. A thorough investigation on the subject, including tests and FEM analysis, was carried out by Yanagisawa *et al* [72]. This research group [77] found that degradation of the epoxy impregnated RE123 coil is eliminated if a polyimide-electrodeposited (PIED) insulation of thickness 15–30 μm is applied to the tape conductor. The transverse stress on the tape is reduced owning to (1) plastic deformation of the ductile polyimide and (2) easily debondable epoxy resin. The polyimide layer acts as a 'missing' soft absorber layer that apparently accommodates thermal mismatches during cool-down. To date, this solution seems to be the best option for insulated coils [78, 79].

Other investigations at UH and Andong University [80, 81] indicate that if the problem must be fixed at the manufacturing stage, a viable solution would be to make the electroplated copper layer thicker, especially along the tape edges, which the slitting may have damaged.

For high-field magnet applications, our focus should be on developing suitable insulation and/or impregnation techniques rather than eliminating defects during the deposition process. All the literature available suggests that in case of epoxy-impregnated coils, it is safer to decouple conductor and epoxy; this decoupling may be unnecessary with PIED insulated tape. The technological consequences of delamination and impregnation are further discussed in section 3.1.3, 'coil impregnation'.

3. Engineering issues in 2G HTS coil technology

3.1. Coil technology

For the HTS magnet to fully achieve its potentials, the intrinsic anisotropic properties of RE123 and large aspect ratio of its tapes pose design challenges, requiring solutions, both innovative and based on the traditional LTS technology. The relevant technical challenges posed by the HTS conductors for magnet applications are winding process, coil impregnation, insulation, and splicing.

3.1.1. Winding techniques.—Two widely used techniques to wind solenoids are layer-wound (LW) and pancake (P)/ double-pancake (DP). In an LW coil, the conductor is wound turn by turn one layer at a time, from the innermost to outermost layers [82]. Generally, the conductor should be long enough to complete at least one full layer. The LW allows the entire coil to be wound with a single conductor piece, provided the conductor is long enough. In a DP coil, applicable to a high- aspect-ratio conductor, e.g., tape, two pancakes are wound sequentially, each pancake starting from the conductor midpoint and spiraling radially outward from the innermost to outermost turns [83]. The 'cross-over' form one pancake to the other at their innermost turns is continuous, i.e., no splice. Because the winding height of each DP coil is about twice the conductor height ($h \geqslant w$, where w is the tape width), a 'long' magnet is an assembly of DP coils. The adjacent DP coils are spliced in the radial space outside the outermost winding diameter. Generally, a DP coil requires a continuous length of conductor that is considerably shorter than that required in a typical LW coil, e.g., even a 50 m long conductor may suffice for a DP coil. Even in a very large magnet, a continuous length of <1 km should be sufficient for a DP coil in contrast to that exceeding 10 km required for an LW magnet. At present, HTS tape longer than 200 m remains a challenging production hurdle, making DP technique a valuable option for HTS

magnet. In this early stage of HTS magnet technology, modularity and scalability, both intrinsic to the DP technique, are attractive features to avoid risks of catastrophic mistakes that may occur during winding and testing. Both LW and DP techniques are being used to wind HTS high-field magnets (see section 4).

3.1.2. Critical aspects of winding.—As extensively discussed in section 2.5, a combination of a thin ceramic biaxially textured RE123 layer and a mechanically tough substrate (Hastelloy, NiW or stainless steel) makes the 2G HTS tape mechanically viable to the high-field magnet, in particular an extremely high axial tensile stress of up to about 700 MPa [84]. Nevertheless, due to a large anisotropic stress tolerance, HTS tapes can be delaminated and degraded by a transversally tensile stress of only 10–20 MPa [72]. In CCs, independent of the fabrication process (RABiTS, IBAD), the superconducting layer is fully formed and present when a coil undergoes the react-and-wind process. In order to preserve the tape's superconducting performances, the conductor strain must be kept below a critical limit. The importance strains are: bending during the winding process [85, 86]; cleavage by differential thermal contractions, particularly in an epoxyimpregnated coil [72]; and electromagnetic hoop stress (see section 3.1.6).

When a coil is wound, the bending strains occur along two principal directions: (a) conductor axis ('easy bending'); (b) normal to the conductor axis ('difficult bending'), at the inner transition region in a double-pancake coil or each end of an LW coil. From the bending analysis of thin beams, Markiewicz *et al* modeled the winding strains of DP and LW coils, derived analytical expressions for the easy and difficult bending strains, and compared their results with the measured irreversible strains [87]. For large winding diameters, bending strains are generally low but become a design constraint for those smaller than 50 mm. Joints are typically located in lowfield regions. Note that, unless a great care is exercised, a great bending strain can occur in a joint [87].

3.1.3. Coil impregnation.—In an LTS solenoid magnet, impregnation (e.g., epoxy, wax [82]) transforms a voidfilled winding into a solid monolithic structure (mechanical load is uniform only in the axial direction), eradicating or minimizing conductor motion, a chief source of premature quenches in nearly all 'adiabatic' LTS magnets in the 1970s and early 1980s. In coils wound with CCs, because of the very large intrinsic temperature margin, the energy released by tape motion is unlikely to induce quenches. Impregnation immobilizes also the conductor against electromagnetic forces —immobilization may prevent stress concentration that results when the conductor moves—and may enhance effective conductive thermal conductivity within the winding, an important benefit especially for coils with a temperature gradient, such as conduction-cooled coils. Nevertheless, at present, most high-field HTS coils are still designed for operation in a bath of liquid He.

The mismatch of the thermal contraction coefficients among former, epoxy and HTS conductors generates thermal stresses that occur mainly around the edge of the conductor [72]. Already in a relatively small pancake coil [76, 88] the thermal stress is enough to induce delamination of the superconducting layer. In the long term the manufacturers of CCs may succeed in developing tapes with improved bonding between the layers, but alternative techniques dealing with the impregnation process of the commercial tapes presently

available have already been reported. For example, in order to avoid the thermal stress at the edge of the conductor, Hwanjun Jeong *et al* [89] suggested reducing the width of the RE123 layer of 30% with respect to the tape width, but this is applicable only to tape which are not slitted after deposition. In general delamination may best be avoided by reducing the adhesion between impregnating material and tape. For the epoxy-impregnated winding, it has been shown that insulating the CC with polyester heat-shrink tubes [75] or electrodeposited polyimide [77] can solve the problem. Another possibility is to modify the coil design: if the magnet is of a nested-coil formation, with each coil's radial build sufficiently thin, the thermal stress is strongly reduced [90].

Another option is to replace epoxy resin with materials of weak bonding strengths. In principle any liquid material that solidifies after the application could be used for filling up voids and obtaining a monolithic structure. For example paraffin and/or bee wax have been used to impregnate CC coil without any major problem [91]. Although several research groups use epoxy impregnation for high-field solenoid coils, epoxy impregnation is not compulsory. Indeed most MRI and NMR magnets are impregnated either with wax or epoxy resin. Another option is cyanoacrylate resin [92], which has also proved to have a sufficiently low adhesion and used successfully for impregnating racetrack coils [92]. One more possibility is to choose a former material of an extremely low thermal contraction that will reduce thermal stress [93].

KIT proposed [94] a blend of araldite epoxy with quartz powder in a 1:1 ratio for degradation-free impregnated RE123 tapes/coils, targeted to Roebel cables. The blend is not the best match with RE123 conductors in terms of thermal contraction from RT to 77 K nor has its effectiveness against delamination been demonstrated with full-scale coils. Furthermore, because the filler generally makes the epoxy denser and more viscous, the epoxy-impregnated DP coils of ⩾4 mm wide superconducting tape are unlikely to be 100% void-free unless the wet winding technique is used.

Finally, it should be pointed out that a coil may also be constructed impregnation-free, i.e., dry winding. Winding tension makes the coil structure a more solid. This is the approach adopted by the NHMFL to construct a 32 T magnet (see section 4).

3.1.4. Coil insulation.—Finding suitable insulation for coils wound with a large aspect ratio tape such as the CC is very challenging. It must operate under severe conditions typical of a superconducting magnet: cryogenic temperatures; large electromagnetic stresses; high voltages developed during quenching. Different techniques have been adopted in prototype HTS magnets depending on their tape, geometry and manufactory method. The Bi2223 manufacturer has proposed Kapton, the 'traditional' insulator for Bi2223 tapes: a thin Kapton tape with or without adhesive is wrapped around the Bi2223 tape, with an overlap that could be specified by the customer. The CC manufacturer has also proposed Kapton. Kapton, weak mechanically, has one additional disadvantage: its thickness is comparable to the CC's. It thus nearly halves the overall current density of the DP coil. As the outer layer of CCs is in general of copper, Kapton may be replaced with enamel [95], a widely used insulation for the NbTi wire. To avoid degrading the coated superconductor, a caveat in applying enamel to the superconductor is to keep its curing temperature below 300 °C and

limit the duration to a few minutes. At IRL [96] a UV curable varnish insulates slitted strands used for Roebel cable. At NHMFL different insulation techniques have been tested, among them thermally-cured and UV-cured polymer coatings, oxide physical vapor deposition, and (on co-wound steel tape) oxide sol-gel coating: a production system of UVcured epoxy coating and an experimental sol-gel coating system have been successfully set up [97]. Other interesting approaches reported are the polyester heat-shrink tubing of Trociewitz *et al* [75] and the electro-deposited polyimide insulation of Yanagisawa [77], both described in section 2.5.3.

In double-pancake coils the tape may be insulated only on one side (layer-to-layer insulation by mean of co-winding an insulating tape), with solid spacers providing the insulation between pancakes. At NHMFL each double pancake of the 32 T magnet is co-wound, without impregnation, with sol-gel alumina-coated stainless steel tape. Considering a low radial thermal conductivity of the pancakes, Bai *et al* [98] suggested that copper cooling disks may be required to promote radial heat flow. BNL also investigated co-winding with bare SS tape and concluded that the low electrical conductivity of steel is sufficient to provide turn-to-turn electrical insulation [99, 100]. The pancakes are dry wound but the top and bottom sides are coated with epoxy before, which is an interesting solution to provide mechanical reinforcement and it may be usueful for quench protection. Weijers *et al* isolated the DP by co-winding with insulated steel, and subsequently vacuum impregnating with unfilled Stycast 1266 epoxy [97]. A 25–50 μm thick Kapton layer separated the pancake halves. When the pancakes were stacked and mounted on the bore tube, the selected units were coated with Stycast 2850 at the i.d. and top/bottom surfaces. Yu *et al* used 0.05 mm thick, 12.7 mm wide Kapton for turn-to-turn insulation for 0.1 mm thick, 12 mm wide RE123 tape. Each turn of the coil has one layer of the Kapton co-wound at the bottom of the superconductor, thus the fraction of the cross-section occupied by the insulation is about 34% [101].

The CC manufacture is currently developing a substitute for Kapton, and the conductor with alternative insulation may become available within next a few years.

The production of no-insulated coils (see section 3.2.1) is being investigated extensively in the last few years. It might be a viable option, if the presence of interlayer electrical resistances is not detrimental to operation. Important operational issues for no-insulated coils include magnet charge sequence, quench protection, and fault-mode unbalanced forces.

3.1.5. Splicing.—Because not only the commercially available CC is currently limited to lengths less than ~300 m but also a magnet comprising an assembly of double-pancake coils requiring many joints, a splicing technique, low-resistance, easy-to-make, and reliable, is required. In LTS materials (NbTi and Nb_3Sn wires) techniques to make superconducting joints are now widely available. The ceramic nature of CCs and their extreme sensitivity to oxygen and high temperatures preclude typical metallurgical jointing approaches, proven successful with LTS. To date, a technique developed recently by Y J Park *et al* [102] gives encouraging results. This approach consists in sintering two counter-facing ceramic layers in vacuum (>800 °C) and restoring the optimal oxygen content by a special heat-treatment performed at a lower temperature. The high-temperature process is short but the annealing

process to re-inject oxygen in the conductor is quite long, over 200 h. Haigun Lee has recently shown that the reoxygenation of Y123 during annealing can be facilitated by opening micro-holes on the surface of the tapes with a laser beam. This approach has been successful in restoring the full I_c of the tape after the jointing process: A current of ~60 A induced at 77 K in a loop containing a joint remained at the same current after more than 200 days [103]. For a magnet comprising double pancake coils, making each joint between adjacent double pancake coils superconducting is a must for persistent-mode operation. Non-superconducting joints can have more flexible geometries, including the lap joint, where two end faces are butt-joined, and the bridge joint, where two HTS tapes are bridged (see figure 7). The electrical resistance of a soldered joint depends on such factors as HTS tape lamination (brass or copper), solder material and layer thickness, surface cleanliness, contact uniformity, and pressure at the time of soldering. The solder resistivity, because solder is an alloy, does not decrease more than a factor of 2 from 77 K and 4.2 K. Another important point with the CC is that the 'superconductor side' surface rather than the 'substrate side' surface must be soldered.

Splicing method, solder material and flux, temperature must match the specific characteristic of the tape: in laminated tape the temperature should be sufficiently low to avoid dismembering the laminated tapes (AMSC and Fujikura RE123; Sumitomo Bi2223). Furthermore, RE123 is deteriorated, by losing oxygen, when heated for a period of time, e.g., >1 min at 300 °C. These inherent dangers are reflected in the soldering recommendations of major manufacturers such as AMSC and SuperPower [104].

Among many reports on preparation of resistive joints, one of the most complete is Duckworth *et al* [105]. Various solders and fluxes were tested for RE123 joints in several configurations. The best results are achieved with twocomponent alloys, e.g., SnAg, InSn, SnPb, with RE123 pretinned or with an aluminium heater block to press the joint surfaces during the soldering process. The specific resistivity, defined as the resistance times the joint area, is a useful parameter. In general, measured specific resistivity at 77 K ranges <30 nΩ cm^2 to >500 nΩ cm^2 [106].

Ko *et al* report results of lap joint and bridge joint that connects two parallel conductors [107]. Of the bridge joint, there are two types, parallel direction (PD joint) and orthogonal direction (OD joint), depending on the direction of the 'bridge' tape with respect to the direction of the parallel CC tapes. The HTS layers of CC tapes faced each other with 75% of each CC tape covered with the bridge tape, as illustrated in figure 8. With a soldering machine developed by themselves [108], they made each joint at 190 °C, pressing it at a pressure of 17 kg mm^{-2}, and cooled it down to room temperature in 15 min [95] Their bridge joint (240 mm^2) contact resistivity and critical current range, respectively, 96–336 nΩ cm^2 and 90–100 A. Although in general, PD joints were better than OD joints, in terms of performance (contact resistivity and critical current) either type fares less well compared with the lap joint.

In section 2.5, the effect of mechanical loads on bare tape performance was discussed in detail. For practical applications splices are absolute necessity. The splices are also subjected to electromagnetic forces. The force on splices has been investigated with techniques similar

to those used to characterize single bare tapes [109, 110]. These studies have shown that the splice's tensile strength may be strongly influenced by the tape architecture. In fact soldered splices without copper stabilizer do not carry full critical currents [109]. Encouragingly, splices of copper-stabilized tapes carry full critical currents up to about 0.5% strain [110]. The source of failed splices is generally the same as that identified in bare tapes: at the interface between buffer layer and RE123. For this reason, strategies that reduce stress peaks at the splice and vicinity may enhance the mechanical properties of the splice.

Independently from the tape architecture (i.e. with or without copper stabilization) it has been demonstrated that the soldered splice resistance is robust and independent of tensile stress.

3.1.6. Stress management.—The use of CCs in high-field superconducting magnets requires high strength against electromagnetic forces. In solenoidal magnets the hoop stress is tensile along the longitudinal direction of the conductor. Since the current carrying capabilities of these ceramic films are strain sensitive, it is necessary to limit the conductor strain. The conductor substrate metal should be strong enough (a high elastic modulus and a large elastic strain limit) to bear most of the hoop stress to limit the strain on the superconducting film. From a conductor point of view, the reinforcement options are described in section 2.5. Examples of peak stresses in high field magnets are reported in section 4.

If the hoop stress is to exceed the substrate strength (or more in general the composite conductor strength, as the tensile stress can also be partially supported by the stabilizer or by the metal tape laminated on the conductor), then an additional reinforcement element must be provided.

Co-winding a high-strength strip is an often-used reinforcement technique. The added material reduces the winding pack overall current density, but allows the conductor to safely carry full operating current. Each design, however, is a comprise among competing requirements. An example is the double pancake design for the 32 T project at NHMFL [111], where an insulated steel tape is co-wound with the superconductor. Alternatively, the overwrap can be entirely wound over individual double-pancake coils, an example of which is a 100 T all-superconducting magnet [112].

For magnets designs not requiring high spatial field homogeneity, other stress management designs are possible. For an SMES unit, Nagaya *et al* [113] are developing the 'Yoroi-coil' structure, where a part of the electromagnetic force is shifted from the conductor to the reinforcing outer plates situated at the side of the coil (figure 9). Using the Yoroi-coil structure concept, they demonstrated that it would be possible to push a calculated magnetic hoop stress of a 100 μm thick Hastelloy-backed conductor to beyond 1.6 GPa versus a typical conductor limit of 1.3 GPa [114]. The measured conductor strain of this test coil was just 0.4%, suggesting that it would be possible to reach magnetic hoop stresses above 2 GPa without any irreversible degradation of the RE123 film. This concept seems to be better suited to pancake magnets, but it should be possible to apply this concept to other coil configurations.

As a final remark, given the inconsistency between tests conducted on straight samples and tests conducted with applied electromagnetic forces on one-turn coils [114], it is possible to argue that the peak hoop stress limit for CC has yet been precisely established and therefore it is recommended that the magnet designer be careful in pushing these conductors close to their mechanical limits.

3.2. Quench protection

As in most devices, the superconducting magnet must be protected against fault mode that may lead to permanent damage. One common fault mode, particularly among LTS magnets, is a quench. The first step in quench protection is the detection of a quench, the most widespread detection technique being the resistive voltage that results from the quench. For a driven-mode magnet, the protection phase consists of two events: first switching off the power supply; and second automatically dumping most of the stored magnet energy into an external ‘dump’ resistor, thereby to keep the initial hot spot from being overheated. The various protection options are discussed in [82]. In the so-called self-protecting magnet the stored energy is dissipated within the magnet winding without external intervention. In case of passive protection, common among persistent-mode, adiabatic LTS magnets, the protection system is within the cryostat: typically diodes and shunt resistors are paralleled across the nested coils comprising a magnet. Examples include laboratory as well as NMR and MRI magnets. In another active protection system, quench heaters placed within the winding are activated to intentionally quench a large enough winding volume, again, to keep the hot spot from being overheated.

One issue in protection of adiabatic coils is the normal zone propagation velocity (NZPV), which in the HTS winding is much slower, by one to two orders of magnitude, than in the LTS winding [115–117]. This is because at a given operating current and magnetic field the NZPV is inversely proportional to the square root of the temperature margin, which is clearly much larger than in classical LTS materials. Adiabatic LTS coils are usually operated very close to the critical surface, i.e. their smallest temperature margins within the winding are often a fraction of a kelvin. When a normal zone appears in the adiabatic LTS winding it will spread very quickly along a large section of the coil. In the HTS winding, because of its low NZPV, the voltage across a normal zone will be low, making quench detection challenging in general and protection in particular [82].

The NZPV and minimum quench energy (MQE) have been measured for CCs test coils in the temperature range 30–80 K (mainly for power applications), but the data are of limited interest for high-field magnets operating at liquid helium temperatures. Measurements on short CC samples at 4.2 K were carried out and the results compared with those for Bi2212 and MgB_2 conductors [118]: at the same reduced current (I/I_c) the NZPV and MQE of CCs and Bi2212 wires are comparable (for example about 40 mm s^{-1} at I/I_c =0.6 and about 100 mm s^{-1} at I/I_c =0.8), while for MgB_2, which has a critical temperature of 39 K, considerably lower than those of RE123 and Bi2212, the respective values are 20 times faster and 5 to 20 times lower.

A very interesting approach to speed up the NZPV in CCs is based on increased contact resistance between the superconducting layer and the stabilizer/substrate [119]. Indeed the

interface next to the superconducting layer appears to be a key player in NZP [120]. The numerical simulation of Badel *et al* [119] shows a drastic increase of NZPV when the thermal conductance of the superconductor/substrate interface becomes lower than 40 W K $^{-1}$ cm^{-1}, i.e. when the superconducting layer is almost thermally decoupled from the substrate. Similarly Levin *et al* proposed [121], on the basis of numerical simulations, that increasing superconductinglayer/stabilizer contact resistance would increase NZPV. Following these indications the modification of an industrial tape from Superpower was carried out by Lacroix *et al* [122]: the superconductor layer is separated from the Ag and Cu layers with a proprietary layer, deposited before the metal matrix layers. The dramatic effect of this layer may be seen from a graph of 77 K NZPV versus current plots on selected contact resistances, shown in figure 10. One drawback is an added, and perhaps more complicated, manufacturing step. Another is reduced stability. Still, it may be worth paying these prices of reduced stability, though the efficacy of this higher contact resistance should further be proved at LHe temperatures in coils rather than only on short samples. In another effort to speed up NZPV, which is a complete opposite of the above, the thermal conductivity within the coil pack was improved with a coat of ZnO [123]. The results were negative with epoxy-impregnated coils, possibly because epoxy might have degraded the overall thermal conductivity. In a more recent experiment [124] titania-doped electrical insulation led to a 2.5 factor increase in NZPV.

With respect to quench detection, optical fibers are used to detect a quench-induced temperature rise [125]. An electromagnetic method involving a special preparation of the tape [126] and acoustic emissions (AE) [127–132] have also been investigated. Except AE technique, which has proven valuable and applied to diagnose the quench sources in adiabatic LTS magnets, the other approaches remain in R&D stage.

One important aspect that should be mentioned is that in the design of LTS magnets the amount of stabilizer (in general copper) is an important parameter, which is optimized for each magnet. In contrast with this, the copper cross-section in the commercial CC is much smaller than those in LTS wires. For example, in the standard 4 mm wide SuperPower CC with 20 μm thick plated copper layers, the total copper crosssection is 0.16 mm^2; since the tape can carry more than 200 A in a high field at 4.2 K, the copper current density can exceed 1000 A mm^{-2}. For comparison, the copper current density in a Nb_3Sn laboratory magnet is less than 300 A mm^{-2}. Ishiyama et al, worked out general equations to estimate the optimal stabilizer cross-section for a SMES magnet operated at 50 K [133]. Regarding high-field coils, simulation study by Uglietti and Marinucci has shown that a moderate increase in copper cross-section coupled with a sensitive quench detection and a short discharge time constant are sufficient to passively protect a 4 T/40 mm bore magnet [134]. For large coils the copper cross-section should be further increased if a passive protection system (shunt resistors with diodes) is used.

Active quench protection often uses heaters. When a quench is detected, the heaters placed within the winding are activated, either by an external power supply or by a portion of the stored energy, quickly driving a large volume of the winding into the normal state. This normal-state volume is generally designed to dissipate the entire stored energy with a limited temperature rise. The quench-inducing heater will be necessary for the HTS coil because of

its low NZPV. Dixon *et al* used a heater system in combination with diodes and resistors to protect a 900 MHz NMR magnet comprising NbTi and Nb_3Sn coils [135]. A heater-based active protection is more complicated to implement, both in design and construction, compared with a passive protection, but it is mandatory, especially for large HTS magnets. A heater-based quench protection system was tested on a Bi2212 insert coils [136]: the experiment shows that this solution is compatible in terms of response time with the protection system of the outer LTS coils. General considerations about protection heaters for CC coils are presented in [137] where heaters are designed for various coil sizes and operating temperature: in general a dense array of heaters is effective for all the cases presented in the paper. A practical application of these considerations is presented in [138] for the protection of a 32 T magnet under construction at the NHMFL (see section 4): quench tests of the double pancake modules were carried out to demonstrate that the 32 T magnet would be safely protected.

3.2.1. No-insulation (NI) coils.—In a very different approach to quench protection, turn-to-turn electrical insulation is removed, completely or partially, to enable the current to flow into the adjacent turns and thereby keep the hot spot from overheated. An Nb_3Sn LW coil with partial insulation (layers insulated, no turn-to-turn insulation) was tested in 1986 [139] and the first NI coil in 1999 [140]. This NI coil consisted of an NbTi cable-in-conduit conductor, which was directly soldered to the coil mandrel to form a detector magnet; in case of quench the current is shunted through the steel conduit. A new detector magnet based on the same design principle was constructed in 2008 [141]. The NI winding technique has also been applied to HTS doublepancake coils wound with Bi2223 and RE123 [142]. Tests at 77 K with these coils demonstrated that the NI coils can withstand over 2.5 times the coil critical current without burning, while insulated coil are very quickly damaged as soon as the critical current is exceeded. Investigation on NZPV was carried out with distributed thermocouples and voltage taps [143].

With CCs measurement at 4.2 K of a single pancake (25 mm i.d., 53 mm o.d., see figure 11) confirmed an exceptional tolerance to over-current: the pancake fully quenched at 486 A and such a high current was maintained for over 30 s [144] (see figure 12). The tape connecting the coil to the copper electrode burned out (see dashed region in figure 11), but measurements at 77 K showed that the coil itself was not damaged. Therefore the authors have suggested that a non-insulated coil should be regarded as a selfprotecting coil, which does not need neither active nor passive protection, i.e. the stored energy can be dissipated in the coil winding without any other circuit or device. An additional benefit is that by removing the insulation and possibly decreasing the stabilizer thickness, the overall coil current density can be further increased.

The main drawback of the NI winding technique is a charging delay time when an NI coil is energized. An NI coil may be modeled with an equivalent LR electric circuit with L given by the coil inductance and R by the turn-to-turn resistance [145]. In the LW coil the delay time constant becomes too long to make the coil impractical [146], unless the coil incorporates partial-insulation winding technique [139, 147].

3.3. Field quality

The field quality is a very important feature of a superconducting magnet. Field quality includes two aspects: temporal stability; and spatial homogeneity (about the magnet center). The field quality for NMR and MRI magnets are much more stringent than that for standard laboratory magnets. For example, an NMR magnet may require a temporal field stability of better than 0.01 ppm h^{-1}, which, for a 20 T magnet, corresponds to a variation of 1.5 mT per year. The tolerance on coil geometry is a key parameter for meeting the spatial homogeneity requirements. This is one reason why LW construction is preferred to pancake construction for MRI and NMR magnets, even with tape conductors.

The field quality of a magnet is degraded, among other factors, by the magnetization of the magnet's superconductor. Based on Bean's model, the magnetization is a result of a screening current induced in the superconductor in response to a time-varying field. In a tape-wound magnet, the radial component of a magnetic field will induce large superconducting screening current loops in the tape [148]. The situation is schematically shown in figure 13. The magnetic field generated by the screening currents is also called shielding field, field error or magnetization.

The screening-current field (SCF) is responsible for: (1) field reduction with respect to the design value; (2) remnant field after the magnet has been discharged; (3) temporal field drift at constant operating current (or in persistent mode) by flux creep. The SCF varies along the magnet axis, thus affecting also the field homogeneity. Some of the very first superconducting solenoid magnets built in the 1960s were wound either with V_3Ga tape or Nb_3Sn tape, whose geometry and architecture are similar to those of modern CCs. Indeed those magnets exhibited a reduced central field, a sizable remnant field after discharge, and large temporal field drift (at constant operating current) [149–151]. Since the beginning of the 1970s multifilamentary wires (NbTi and Nb_3Sn) have become the standard in the industry. Because of the fine filaments (2–100 μm) the screening current loops are very small, making their SCF negligible. Nevertheless for NMR and MRI magnets, filaments should be as fine as possible (typical Nb_3Sn Bronze Route wires for NMR magnets have filaments diameters betwen 2 μm and 5 μm). The detrimental effects of SCF on field quality were observed in the first decade of this century, when Bi2223 tapes were used to build inserts for NMR magnets [152, 153]. In [154] and [155] the SCF of the Bi2223 insert was found to be responsible for reduction in the total magnetic field, a large gradient in the harmonic components, and large temporal drift (field decay). Although Bi2223 tape, unlike CC tape, consists of many filaments, because the filaments are embedded in silver matrix and thus electromagnetically coupled, its SCF is large.

SCF will be even larger in CC, which basically consists of a single monofilament (the superconducting layer) of width in the range 3–12 mm: this is about three orders of magnitude larger than the finest filaments in Nb_3Sn wires. It follows that the detrimental effects of SCF on field quality should also be larger in the same order. A detailed calculation of SCF in CC coils (see figure 14) was carried out at LHe temperature [156]. It was found that the center field ratio of the SCF to the coil is maximum for a minimum-volume coil, whereas it is much lower for short-and-thick (pancake) coils and long-and-thin coils. For a fixed aspect ratio, for example, a minimumvolume coil, the ratio first increases with coil

volume, reaches a maximum, and then decreases (see figure 15). Moreover, for a fixed coil shape, SFC is proportional to the ratio of tape width to coil i.d. [157]. Of course, minimum-volume coil is generally unsuitable to meet high spatial field homogeneity requirements.

The detrimental effects of SFC on field for an all-coatedconductor 1.3 GHz NMR magnet have been evaluated numerically [158]: at the center the SFC would reduce the strength by ~8% and deteriorate the spatial homogeneity. Even if NbTi correction coils are placed at magnet ends, they are ineffective to improve the field homogeneity.

Field reduction and remnant field were measured for coils of different aspect ratios [159]; measurement and computation ([157]) agree quite well. The field temporal stability in a small coil of the same aspect ratio as that of a nominal-size NMR coil was measured; the small coil was found to have a temporal drift of 10 ppm h^{-1}, clearly much greater than that for a typical NMR operation [159]. One technique proposed recently to shim SFC-induced field impurity is a set of persistent-mode shim coils prepared from RE123 [160].

Despite a report of a superconducting joint between coated superconductors (see section 3.1.5), a persistent-mode NMR magnet of CC could still be difficult because of the temporal drift due to the screening currents. Various techniques have been proposed to reduce the amplitude of the screening currents. These possible techniques include: multifilamentary CCs (striated CCs, see section 2.4) would reduce SCF inversely to the number of filaments, for example, with 10 filaments, SCF would be reduced by 10; the so-called overshooting technique [161], though not really useful for the NMR magnet, reverses a current sweep, as small as 1% of the peak current, to impede SCF variation; apply a field parallel to the tape wide surface with copper coils that sandwich a CC coil [162].

4. Overview on ongoing high-field DC magnet projects based on RE123

The progress of high-field magnets has tracked closely the advancement of superconductors and materials science. It has been propelled by new frontiers of science and science-driven innovation in which a magnetic field plays a key role. The trends and driving forces for these ambitious high-field magnets are summarized in a 2013 report by the National Academy of Sciences [163]. Among new ideas, recommendations, future technological objectives, the report recommends the construction of a 40 T all-superconducting DC magnet that should motivate research institutions in the world active in superconducting magnet technology.

In this section we present selected steady (DC) all-RE123 high-field solenoids, the main design parameters of which are given in table 4.

The highest magnetic field ever achieved, 35.4 T, was obtained with a 4.2 T insert wound with 96 m long RE123 in a 31.2 T resistive outsert at the NHMFL [75]. The RE123 insert incorporates an innovative insulation material of nonbonding thin polyester film that prevents conductor degradation during cooling (see sections 2.5.3 and 3.1.3).

An important project that has been upgraded along the course of the years is a 1.3 GHz (30.5 T) NMR magnet under construction at the MIT Francis Bitter Magnet Laboratory [164]. The magnet is particularly interesting, and challenging, because it fully capitalizes the high-field

potential of RE123, making the RE123 insert, despite stringent NMR-quality field requirements, contribute 800 MHz, over 60% of the total frequency (and field). Upon successful completion, this magnet will become a power tool for advancement in biomedical sciences [163]. This 500 MHz LTS/800 MHz RE123 combination superseded a 600 MHz LTS/700 MHz HTS (Bi2223/RE123) combination [165], which had earlier replaced yet another combination of a 700 MHz LTS/ 600 MHz HTS (Bi2223/RE123) [166]. Two of the most remarkable features of this design are related to the insulation strategy and field quality. In fact a NI winding technique is adopted in order to make the 800 MHz RE123 insert selfprotecting without adding extra Cu stabilizer, compact, and mechanically robust. Despite its rather short overall winding length, its computed field quality, in the absence of SCF, is maintained with inside-notched central DP coils [164].

Another high-field NMR system is being developed at NIMS, Tsukuba, in Japan, in which the goal is to go beyond 1 GHz [167, 168]. The project is going through several intermediate stages to develop RE123 magnet technology. Currently their focus is on a 600 MHz RE123 system. For this purpose they tested in 2011 a short LW 7.6 T RE123 insert in a background LTS field of 17.2 T [169]. An interesting feature introduced in this test coil is a resistive joint connecting the two 250 m long RE123 sections. The splice, embedded within the coil winding, was operated successfully up to 321 A. Although the coil design was quite conservative in regard to a maximum stress (460 MPa) its copper current density was quite ambitious (960 A mm^{-2}), requiring a reliable protection system.

In terms of laboratory high-field magnets targeting materials science and solid-state physics research, a 32 T magnet project at NHMFL deserves a special citation: today this project is one of the most advanced, incorporating allLTS and HTS coils in a unique high-field facility (figure 16) [111, 170]. The program has a stated double purpose of enabling unprecedented high-field research activities and demonstrating HTS-based magnet technologies. The design parameters for this magnet, aimed to serve the user for 20 years, focuses on modularity and generous operating margins. The hoop-stress is limited to 450 MPa on RE123 conductor and copper current density to 440 A mm^{-2} to ease protection requirements. These rather conservative choices, taken to ensure reliability and longevity, pose challenge, particularly for RE123 insert. The total RE123 conductor length is almost 10 km, configured into 56 double-pancake coils, each wound with special insulation and reinforcement mechanism, and protected [171].

It is interesting to note that for some of these projects there has been a shift from hybrid Bi2223-RE123 coil formation toward all-RE123 formation [164, 166, 172–174]. This shift may reflect the RE123's steady performance improvement in electromagnetic properties and its inherent mechanical strength advantage over Bi2223. Based on the design parameters listed in table 4, it appears that the adopted stress management strategies even under severe operating conditions are consistent with the well-known RE123 properties. On the other hand, there still remains a wide range of protection strategies, from the self-protecting feature of the NI winding technology to the traditional protection techniques for insulated winding technology. This protection issue will certainly be subject of deeper investigations and debate in the near future when these projects will enter in their critical production and testing phases.

In parallel to the high-field NMR project the High Field Laboratory for Superconducting Materials (HFLSC) in Sendai is also planning an upgrade to their 18 T cryogen-free superconducting magnet (CSM). The proposed field target of 25 T [172, 173] could be achieved with a 14 T LTS outsert and a single RE123 insert. This RE123 coil also uses quite relaxed parameters, and combined with its large inner bore (96 mm winding diameter), the coil will require RE123 conductor in excess of 17 km.

As a final closing citation in this section dedicated to high-magnetic field systems, a special note is reserved to a 100 T DC magnet proposed recently by Iwasa and Hahn [112]. Their design in fact pushes to the extreme limit all aspects of the RE123 technology and magnet design developed to date. The technological effort will be comparable with those of LHC ATLAS and ITER TF magnets: the 100 T magnet, almost 17 m tall and nearly 6 m outer diameter, stores more than 120 GJ of magnetic energy. It comprises 39 nested all-RE123 coils, assembled from more than 14 000 doublepancake coils requiring a total of more than 12 000 km of 12 mm wide RE123 tape. One of the main enabling ingredients for this ambitious magnet is the RE123 conductor. With its unique electromagnetic properties and mechanical strength, RE123 seems at present the only suitable superconductor. A 100 T DC superconducting magnet, perhaps the Holy Grail of a continuous (DC) magnetic field, is an example of an innovative, and ambitious, design that in order to convert to reality requires a further superconducting magnet technology R&D effort, and surely of an international scale, like ITER and LHC.

5. Conclusions

Currently, because of its current-carrying capacity and, equally importantly, high mechanical strength, RE123 is the only high-temperature superconductor applicable to high-field magnets. It is unlikely that even continued progress in Bi2212 and Bi2223 conductors will able to resolve their inherent disadvantage in mechanical strength versus RE123. To fully capitalize on the remarkable properties of RE123, a wide range of techniques has been developed and some already successfully deployed. Despite many challenging issues that confront RE123, and the magnet, its demanding and inspiring partner, together they are poised to break through into a new brave high-field world, even unimagined at the beginning of the HTS era. We strongly believe that this new high-field world, where HTS is unquestionably the enabling technology, will lead to major discoveries and development in many areas of physics, biology, chemistry, materials, medicine, and engineering, possibly even entirely original studies that would have been impossible or even inconceivable.

Acknowledgements

CS acknowledge the financial support from the Swiss National Science Foundation (Grant No. PP00P2_144673 and 51NF40–144613).

References

[1]. Wu MK, Ashburn JR, Torng CJ, Hor PH, Meng RL, Gao L, Huang ZJ, Wang YQ and Chu CW 1987 Superconductivity at 93 K in a new mixed-phase Y−Ba−Cu −O compound system at ambient pressure Phys. Rev. Lett 58 908–10 [PubMed: 10035069]

[2]. Maeda H, Tanaka Y, Fukutomi M and Asano T 1988 A new high-T_c oxide superconductor without a rare-Earth element Japan. J. Appl. Phys 2 L209–10

[3]. Larbalestier DC et al. 2014 Isotropic round-wire multifilament cuprate superconductor for generation of magnetic fields above 30 T Nat. Mater 13 375–81 [PubMed: 24608141]

[4]. Iijima Y, Tanabe N, Kohno O and Ikeno Y 1992 Inplane aligned Yba2cu3o7−x thin-films deposited on polycrystalline metallic substrates Appl. Phys. Lett 60 769–71

[5]. Graser S, Hirschfeld PJ, Kopp T, Gutser R, Andersen BM and Mannhart J 2010 How grain boundaries limit supercurrents in high-temperature superconductors Nat. Phys 6 609–14

[6]. Hilgenkamp H and Mannhart J 2002 Grain boundaries in high-Tc superconductors Rev. Mod. Phys 74 485

[7]. Lehner T 2012 Investigation of HTS materials for electric power equipment Workshop on Present, Status Future Perspectives of Hts Power Applications (Paris, France) www.superpower-inc.com/system/files/2012_0829+CIGRE+WS+Pres_Lehner_HTS+Materials+FINAL.pdf)

[8]. Goyal A et al. 1997 Conductors with controlled grain boundaries: an approach to the next generation, high temperature superconducting wire J. Mater. Res 12 2924–40

[9]. Groves JR, Arendt PN, Kung H, Foltyn SR, DePaula RF, Emmert LA and Storer JG 2001 Texture development in IBAD MgO films as a function of deposition thickness and rate IEEE Trans. Appl. Supercond 11 2822–5

[10]. Rupich MW et al. 2004 Progress on MOD/RABiTSTM 2G HTS wire Physica C: Supercond 412–414 877–84

[11]. Nagaishi T, Shingai Y, Konishi M, Taneda T, Ota H, Honda G, Kato T and Ohmatsu K 2009 Development of REBCO coated conductors on textured metallic substrates Physica C: Supercond 469 1311–5

[12]. Rupich M. et al. 2010; Advances in second generation high temperature superconducting wire manufacturing and R&D at american superconductor corporation. Supercond. Sci. Technol. 23:014015.

[13]. Rupich MW, Li X, Sathyamurthy S, Thieme CLH, DeMoranville K, Gannon J and Fleshler S 2013 Second Generation wire development at AMSC IEEE Trans. Appl. Supercond 23 6601205

[14]. Suo H, Zhao Y, Liu M, Ma L, He D, Zhang Y and Zhou M 2007 Preparation of cube textured Ni5W/Ni9W composite substrate for YBCO coated conductors IEEE Trans. Appl. Supercond 17 3420–3

[15]. Oh SS. et al. 2008; Development of long-length SmBCO coated conductors using a batch-type reactive coevaporation method. Supercond. Sci. Technol. 21:034003.

[16]. Igarashi M. et al. 2010; Remarkable progress in fabricating RE123 coated conductors by IBAD/PLD technique at fujikura. J. Phys.: Conf. Ser. 234:022016.

[17]. Dong L and Srolovitz DJ 1998 Texture development mechanisms in ion beam assisted deposition J. Appl. Phys 84 5261–9

[18]. Igarashi, M; RE123 coated conductors Fujikura Technical Review No.38. 2009. www.fujikura.co.jp/eng/rd/gihou/backnumber/pages/1198117_4995.html

[19]. Xiong X, Kim S, Zdun K, Sambandam S, Rar A, Lenseth KP and Selvamanickam V 2009 Progress in high throughput processing of long-length, high quality, and low cost IBAD MgO buffer tapes at superpower IEEE Trans. Appl. Supercond 19 3319–22

[20]. Lee S, Petrykin V, Molodyk A, Samoilenkov S, Kaul A, Vavilov A, Vysotsky V and Fetisov S 2014 Development and production of second generation high T-c superconducting tapes at superox and first tests of model cables Supercond. Sci. Technol 27 044022

[21]. Usoskin A, Kirchhoff L, Knoke J, Prause B, Rutt A, Selskij V and Farrell DE 2007 Processing of long-length YBCO coated conductors based on stainless steel tapes IEEE Trans. Appl. Supercond 17 3235–8

[22]. Matias V, Rowley J, Coulter Y, Maiorov B, Holesinger T, Yung C, Glyantsev V and Moeckly B 2010 YBCO films grown by reactive co-evaporation on simplified IBAD-MgO coated conductor templates Supercond. Sci. Technol 23 014018

[23]. Malozemoff AP. et al. 2008; Progress in high temperature superconductor coated conductors and their applications. Supercond. Sci. Technol. 21:034005.

[24]. Selvamanickam V et al. 2000 High-current Y–Ba–Cu–O superconducting films by metal organic chemical vapor deposition on flexible metal substrates Physica C: Supercond 333 155–62

[25]. Watanabe T, Kuriki R, Iwai H, Muroga T, Miyata S, Ibi A, Yamada Y and Shiohara Y 2005 High rate deposition by PLD of YBCO films for coated conductors IEEE Trans. Appl. Supercond 15 2566–9

[26]. Usoskin A, Knoke J, Garcia-Moreno F, Issaev A, Dzick J, Sievers S and Freyhardt HC 2001 Large-area HTS-coated stainless steel tapes with high critical currents IEEE Trans. Appl. Supercond 11 3385–8

[27]. Van Driessche I. et al. 2012; Chemical solution deposition using ink-jet printing for YBCO coated conductors. Supercond. Sci. Technol. 25:065017.

[28]. Obradors X, Puig T, Ricart S, Coll M, Gazquez J, Palau A and Granados X 2012 Growth, nanostructure and vortex pinning in superconducting YBa2Cu3O7 thin films based on trifluoroacetate solutions Supercond. Sci. Technol 25 123001

[29]. Christen HM and Eres G 2008 Recent advances in pulsedlaser deposition of complex oxides J. Phys.: Condens. Matter 20 264005 [PubMed: 21694339]

[30]. Ma B, Koritala RE, Fisher BL, Uprety KK, Baurceanu R, Dorris SE, Miller DJ, Berghuis P, Gray KE and Balachandran U 2004 High critical current density of YBCO coated conductors fabricated by inclined substrate deposition Physica C: Supercond 403 183–90

[31]. Moon SH. 2013SuNAM developed new process named RCE-DR: the practical highest throughput process 11th European Conf. on Applied Superconductivity EuCAS.

[32]. Moon SH 2014 HTS development and industrialization at SuNAM. 1st Workshop on Accelerator Magnets in HTS (Hamburg, Germany) http://indico.cern.ch/event/308828/session/2/contribution/10/material/slides/1.pdf)

[33]. MacManus-Driscoll JL, Foltyn SR, Jia QX, Wang H, Serquis A, Civale L, Maiorov B, Hawley ME, Maley MP and Peterson DE 2004 Strongly enhanced current densities in superconducting coated conductors of $YBa_2Cu_3O_{7-x}$+$BaZrO_3$ Nat. Mater 3 439–43 [PubMed: 15170180]

[34]. Chen Y, Selvamanickam V, Zhang Y, Zuev Y, Cantoni C, Specht E, Paranthaman P, Aytug T, Goyal A and Lee D 2009 Enhanced flux pinning by BaZrO3 and (Gd,Y)2O3 nanostructures in metal organic chemical vapor deposited GdYBCO high temperature superconductor tapes Appl. Phys. Lett 94 062513

[35]. Gutierrez J et al. 2007 Strong isotropic flux pinning in solution-derived YBa2Cu3O7−x nanocomposite superconductor films Nat. Mater 6 367–73 [PubMed: 17450145]

[36]. Matsushita T. et al. 2012; Improvement of flux pinning performance at high magnetic fields in GdBa2Cu3Oy coated conductors with BHO nano-rods through enhancement of Bc_2. Supercond. Sci. Technol. 25:125003.

[37]. Selvamanickam V, Yao Y, Chen Y, Shi T, Liu Y, Khatri ND, Liu J, Lei C, Galstyan E and Majkic G 2012 The low-temperature, high-magnetic-field critical current characteristics of Zr-added (Gd,Y)$Ba_2Cu_3O_x$ superconducting tapes Supercond. Sci. Technol 25 125013

[38]. Miura M, Maiorov B, Baily SA, Haberkorn N, Willis JO, Marken K, Izumi T, Shiohara Y and Civale L 2011 Mixed pinning landscape in nanoparticle-introduced $YGdBa_2Cu_3O_y$ films grown by metal organic deposition Phys. Rev B 83 184519

[39]. Choi SM, Lee JW, Shin GH, Lee JH, Hong GW, Moon SH and Yoo SI 2013 Characteristics of High-J(c) GdBCO coated conductors fabricated by the RCE-DR process IEEE Trans. Appl. Supercond 23 8001004

[40]. Selvamanickam V et al. 2011 Progress in performance improvement and new research areas for cost reduction of 2G HTS wires IEEE Trans. Appl. Supercond 21 3049–54

[41]. Braccini V. et al. 2011; Properties of recent IBAD-MOCVD coated conductors relevant to their high field, low temperature magnet use. Supercond. Sci. Technol. 24:035001.

[42]. Weijers HW 2009 High-temperature superconductors in high-field magnets PhD Thesis University of Twente doi:10.3990/1.9789036528498

[43]. Hahn S, Kim Y, Park DK, Kim K, Voccio JP, Bascunan J and Iwasa Y 2013 No-insulation multi-width winding technique for high temperature superconducting magnet Appl. Phys. Lett 103 173511 [PubMed: 24255549]

[44]. Obradors X and Puig T 2014 Coated conductors for power applications: materials challenges Supercond. Sci. Technol 27 044033

[45]. Rolando G 2013 Cable-in-conduit superconductors for fusion magnets PhD Thesis University of Twente doi:10.3990/1.9789036535632

[46]. Lu J, Choi ES, Kandel H, Abraimov DV and Markiewicz WD 2014 Hysteresis loss of REBCO conductor up to 35 T IEEE Trans. Appl. Supercond 24 8200104

[47]. Kesgin I, Majkic G and Selvamanickam V 2013 Fully filamentized HTS coated conductor via striation and selective electroplating Physica C: Supercond 486 43–50

[48]. Kuhn M, Schey B, Klarmann R, Biegel W, Stritzker B, Eisenmenger J and Leiderer P 1998 Patterning of YBCO thin films by ion implantation and magneto-optical investigations Physica C: Supercond 294 1–6

[49]. Cobb C, Barnes P, Haugan T, Tolliver J, Lee E, Sumption M, Collings E and Oberly C 2002 Hysteretic loss reduction in striated YBCO Physica C: Supercond 382 52–6

[50]. Duckworth RC, Paranthaman MP, Bhuiyan MS, List FA and Gouge MJ 2007 AC losses in YBCO coated conductor with inkjet filaments IEEE Trans. Appl. Supercond 17 3159–62

[51]. Ma QY, Dosanjh P, Wong A, Carolan JF and Hardy WN 1994 Inhibition patterning of oxide superconducting films with Si ion implantation Supercond. Sci. Technol 7 294

[52]. Sunwong P, Higgins JS, Tsui Y, Raine MJ and Hampshire DP 2013 The critical current density of grain boundary channels in polycrystalline HTS and LTS superconductors in magnetic fields Supercond. Sci. Technol 26 095006

[53]. Mondonico G, Seeber B, Senatore C, Flükiger R, Corato V, De Marzi G and Muzzi L 2010 Improvement of electromechanical properties of an ITER internal tin Nb_3Sn wire J. Appl. Phys 108 093906

[54]. Welp U. 1992; Effect of uniaxial stress on the superconducting transition in $YBa_2Cu_3O_7$. Phys. Rev. Lett. 69:2130. [PubMed: 10046406]

[55]. van der Laan DC, Abraimov D, Polyanskii AA, Larbalestier DC, Douglas JF, Semerad R and Bauer M 2011 Anisotropic in-plane reversible strain effect in $Y_{0.5}Gd_{0.5}Ba_2Cu_3O_{7-\delta}$ coated conductors Supercond. Sci. Technol 24 115010

[56]. Sugano M. et al. 2012; The effect of the 2D internal strain state on the critical current in GdBCO coated conductors. Supercond. Sci. Technol. 25:054014.

[57]. van der Laan DC, Lu XF and Goodrich LF 2011 Compact GdBa2Cu3O7−δ coated conductor cables for electric power transmission and magnet applications Supercond. Sci. Technol 24 042001

[58]. van der Laan DC, Ekin JW, Douglas JF, Clickner CC, Stauffer TC and Goodrich LF 2010 Effect of strain, magnetic field and field angle on the critical current density of $YBa_2Cu_3O_{7-\delta}$ coated conductors Supercond. Sci. Technol 23 072001

[59]. Sugano M, Shikimachi K, Hirano N and Nagaya S 2010 The reversible strain effect on critical current over a wide range of temperatures and magnetic fields for YBCO coated conductors Supercond. Sci. Technol 23 085013

[60]. Kinoshita KHTS development and industrialization at Sumitomo 1st Workshop on Accelerator Magnets in HTS (Hamburg, Germany) http://indico.cern.ch/event/308828/session/2/contribution/9/material/slides/1.pdf

[61]. Cheggour N, Ekin JW, Xie YY, Selvamanickam V, Thieme CLH and Verebelyi DT 2005 Enhancement of the irreversible axial-strain limit of Y−Ba−Cu−O-coated conductors with the addition of a Cu layer Appl. Phys. Lett 87 212505

[62]. Shin H-S, Kim K-H, John R, Kim T-Y, Ko R-K and Oh S-S 2005 The strain effect on critical current in YBCO coated conductors with different stabilizing layers Supercond. Sci. Technol 18 S364

[63]. Osamura K, Machiya S, Ochiai S, Osabe G, Yamazaki K and Fujikami J 2013 High strength/high strain tolerance DIBSCCO tapes by means of pre-tensioned lamination technique IEEE Trans. Appl. Supercond 23 6400504

[64]. Shin H-S and Dedicatoria M 2012 Variation of the strain effect on the critical current due to external lamination in REBCO coated conductors Supercond. Sci. Technol 25 054013

[65]. Shin H-S and Dedicatoria M 2013 Intrinsic strain effect on critical current in Cu-stabilized GdBCO coated conductor tapes with different substrates Supercond. Sci. Technol 26 055005

[66]. Uglietti D, Seeber B, Abächerli V, Carter WL and Flükiger R 2006 Critical currents versus applied strain for industrial Y-123 coated conductors at various temperatures and magnetic fields up to 19 T Supercond. Sci. Technol 19 869–72

[67]. Usoskin A. 2011Physical principles and applications of inductive HTS shielded fault current limiting devices with suppressed cryogenic losses. 10th EPRO Conf. (Tallahassee, US).

[68]. Matias V, Jung Y and Sheehan C 2010 Progress in reactive co-evaporation on IBAD Advanced Cables and Conductors Program Peer Review (Alexandria, US) www.htspeerreview.com/pdfs/presentations/day%202/2G/2_2G_Progress_in_Reactive_CoEvaporation_on_IBAD.pdf

[69]. Mbaruku AL and Schwartz J 2008 Fatigue behavior of Y−Ba −Cu−O/hastelloy-C coated conductor at 77 K IEEE Trans. Appl. Supercond 18 1743–52

[70]. Sugano M, Yoshida Y, Hojo M, Shikimachi K, Hirano N and Nagaya S 2008 Two different mechanisms of fatigue damage due to cyclic stress loading at 77 K for MOCVDYBCO-coated conductors Supercond. Sci. Technol 21 054006

[71]. Shin HS and Dedicatoria MJ 2011 Mechanical and transport properties of IBAD/EDDC-SmBCO coated conductor tapes during fatigue loading Cryogenics 51 237–40

[72]. Yanagisawa Y, Nakagome H, Takematsu T, Takao T, Sato N, Takahashi M and Maeda H 2011 Remarkable weakness against cleavage stress for YBCO-coated conductors and its effect on the YBCO coil performance Physica C: Supercond 471 480–5

[73]. Maeda H and Yanagisawa Y 2014 Recent developments in high-temperature superconducting magnet technology (review) IEEE Trans. Appl. Supercond 24 4602412

[74]. van der Laan DC, Ekin JW, Clickner CC and Stauffer TC 2007 Delamination strength of YBCO coated conductors under transverse tensile stress Supercond. Sci. Technol 20 765–70

[75]. Trociewitz U, Canassy M, Hannion M, Hilton D, Jaroszynski J, Noyes P, Viouchkov Y, Weijers H and Larbalestier D 2011 35.4 T field generated using a layerwound superconducting coil made of (RE)$Ba_2Cu_3O_{7-x}$ (RE=rare Earth) coated conductor Appl. Phys. Lett 99 202506

[76]. Takematsu T, Hu R, Takao T, Yanagisawa Y, Nakagome H, Uglietti D, Kiyoshi T, Takahashi M and Maeda H 2010 Degradation of the performance of a YBCO-coated conductor double pancake coil due to epoxy impregnation Physica C: Supercond 470 4

[77]. Yanagisawa Y, Sato K, Piao R, Nakagome H, Takematsu T, Takao T, Kamibayashi H, Takahashi M and Maeda H 2012 Removal of degradation of the performance of an epoxy impregnated YBCO-coated conductor double pancake coil by using a polyimide-electrodeposited YBCO-coated conductor Physica C: Supercond 476 19–22

[78]. Sato K, Matsuda T, Yanagisawa Y, Nakagome H, Kamibayashi H, Uchida A, Takahashi M and Maeda H 2013 The performance of a practical size epoxy impregnated pancake coil wound with a polyimide electro-deposited (PIED) YBCO-coated conductor IEEE Trans. Appl. Supercond 23 4602504

[79]. Maeda H, Takahashi M, Yanagisawa Y, Nakagome H, Oobuchi K and Kamibayashi H 2013 Coated hightemperature superconducting wire and high-temperature superconducting coil including the same European Patent Application 12189570.0 filed 23 October 2012, published 01 May 2013

[80]. Majkic G, Galstyan E, Zhang Y and Selvamanickam V 2013 Investigation of delamination mechanisms in IBADMOCVD REBCO coated conductors IEEE Trans. Appl. Supercond 23 6600205

[81]. Gorospe A, Nisay A, Dizon JR and Shin HS 2013 Delamination behaviour of GdBCO coated conductor tapes under transverse tension Physica C: Supercond 494 163–7

[82]. Iwasa Y 2009 Case Studies in Superconducting Magnets 2nd edn (Berlin: Springer)

[83]. Kim SW, Sohn MH, Baik SK, Jo YS, Seo MG, Lee EY, Ko RK and Kwon YK 2003 Soldered double pancake winding of high temperature superconducting tape IEEE Trans. Appl. Supercond 13 1784–7

[84]. Hazelton DW, Selvamanickam V, Duval JM, Larbalestier DC, Markiewicz WD, Weijers HW and Holtz RL 2009 Recent developments in 2G HTS coil technology IEEE Trans. Appl. Supercond 19 2218–22

[85]. Takao T et al. 2007 Influence of bending and torsion strains on critical currents in YBCO coated conductors IEEE Trans. Appl. Supercond 17 3513–6

[86]. Takao T, Sakabe R, Asano T, Mitsui S, Nakao K, Shiohara Y and Kashima N 2009 Degradation due to bending fatigue strain in YBCO coated conductors IEEE Trans. Appl. Supercond 19 2988–90

[87]. Markiewicz WD and Swenson CA 2010 Winding strain analysis for YBCO coated conductors Supercond. Sci. Technol 23 045017

[88]. Shiroyanagi Y, Ghosh AK, Gupta R and Sampson WB 2011 The construction and testing of YBCO pancake coils for a high field solenoid IEEE Trans. Appl. Supercond 21 1649–52

[89]. Jeong H. et al. 2012; De-lamination characteristics of coated conductor for conduction cooled HTS coil. IEEE Trans. Appl. Supercond. 22:7700804.

[90]. Awaji S. et al. 2013; Superconducting and mechanical properties of impregnated REBCO pancake coils under large hoop stress. IEEE Trans. Appl. Supercond. 23:4600305.

[91]. Uglietti D, Choi S, Matsumoto S and Kiyoshi T 2011 High current density in layer-wound coated conductorcoils Oficyna Wydawnicza Politech. Wroc. (Wroclaw, Poland) 1219

[92]. Mizuno K, Ogata M and Nagashima K 2013 An innovative superconducting coil fabrication method with YBCO coated conductors Q. Rep. Railw. Tech. Res. Inst 54 46–51

[93]. Oomen M, Herkert W, Bayer D, Kummeth P, Nick W and Arndt T 2012 Manufacturing and test of 2G-HTS coils for rotating machines: challenges, conductor requirements, realization Physica C: Supercond 482 111–8

[94]. Barth C, Bagrets N, Weiss KP, Bayer CM and Bast T 2013 Degradation free epoxy impregnation of REBCO coils and cables Supercond. Sci. Technol 26 055007

[95]. Uglietti D, Choi S and Kiyoshi T 2010 Design and fabrication of layer-wound YBCO solenoids Physica C: Supercond 470 1749–51

[96]. Badcock RA, Long NJ, Mulholland M, Hellmann S, Wright A and Hamilton KA 2009 Progress in the manufacture of long length YBCO roebel cables IEEE Trans. Appl. Supercond 19 3244–7

[97]. Weijers HW et al. 2010 High field magnets with HTS conductors IEEE Trans. Appl. Supercond 20 576–82

[98]. Bai H, Markiewicz WD, Lu J and Weijers HW 2013 Thermal conductivity test of YBCO coated conductor tape stacks interleaved with insulated stainless steel tapes IEEE Trans. Appl. Supercond 23 4600204

[99]. Gupta R. 2013High field HTS solenoid for a muon collider demonstrations. Challenges and Strategies Int. Conf. on Magnet Technology MT23 (Boston, USA).

[100]. Gupta R et al. 2011 High field HTS R&D solenoid for muon collider IEEE Trans. Appl. Supercond 21 1884–7

[101]. Yu M, Lombardo V, Lopes ML, Turrioni D, Zlobin AV, Flanagan G and Johnson RP 2011 Test of 1st YBCO helical solenoid double pancake model 2011 Particle Accelerator Conf 1118

[102]. Park Y, Shin H-J, Kim Y-G, Oh Y and Lee H 2013 Effects of melting diffusion and annealing in oxygen on superconducting characteristics of GdBCO coated conductors: preliminary results IEEE Trans. Appl. Supercond 23 6600804

[103]. Park Y, Lee M, Ann H, Choi Y and Lee H 2013 A superconducting joint for GdBa2Cu3O7−δ coated conductors Nat. Asia 6 e98

[104]. www.superpower-inc.com/system/files/SP_Soldering+Instructions_2013FEC_v2.pdf

[105]. Duckworth RC, Zhang Y, Gouge MJ, Rey CM, van der Laan DC and Clickner C 2010 Voltage distribution and mechanical strength in splice joints made from as-manufactured YBCO coated conductors AIP Conf. Proc 1219 370–9

[106]. Kim Y, Bascunan J, Lecrevisse T, Hahn S, Voccio J, Park DK and Iwasa Y 2013 YBCO and Bi2223 coils for high field LTS/HTS NMR magnets: HTS-HTS joint resistivity IEEE Trans. Appl. Supercond 23 6800704 [PubMed: 31130800]

[107]. Chang K, Jo H, Kim Y, CheolAhn M and Ko T 2011 An experimental study on the joint methods between double pancake coils using YBCO coated conductors IEEE Trans. Appl. Supercond 21 3005–8

[108]. Chang K, Park D, Yang S, Jo H, Kim H, Yoon Y, Kim H, Lee H and Ko T 2010 Experimental analysis of a splice method between YBCO coated conductors on various bending diameters IEEE Trans. Appl. Supercond 20 1577–80

[109]. Sugano M, Nakamura T, Shikimachi K, Hirano N and Nagaya S 2007 Stress tolerance and fracture mechanism of solder joint of YBCO coated conductors IEEE Trans. Appl. Supercond 17 3067–70

[110]. Walsh RP, McRae D, Markiewicz WD, Lu J and Toplosky VJ 2012 The 77 K stress and strain dependence of the critical current of YBCO coated conductors and lap joints IEEE Trans. Appl. Supercond 22 8400406

[111]. Markiewicz DW. et al. 2012; Design of a superconducting 32 T magnet with REBCO high field coils. IEEE Trans. Appl. Supercond. 22:4300704.

[112]. Iwasa Y and Hahn S 2013 First-cut design of an allsuperconducting 100 T direct current magnet Appl. Phys. Lett 103 253507 [PubMed: 24399859]

[113]. Nagaya S, Watanabe T, Tamada T, Naruse M, Kashima N, Katagiri T, Hirano N, Awaji S, Oguro H and Ishiyama A 2013 Development of high strength pancake coil with stress controlling structure by REBCO coated conductor IEEE Trans. Appl. Supercond 23 4601204

[114]. Nishijima G, Minegishi K, Awaji S, Watanabe K, Izumi T and Shiohara Y 2011 Hoop stress test of $GdBa_2Cu_3O_y$ coated conductor IEEE Trans. Appl. Supercond 21 3094–7

[115]. Grabovickic R, Lue JW, Gouge MJ, Demko JA and Duckworth RC 2003 Measurements of temperature dependence of the stability and quench propagation of a 20 cm-long RABiTS Y−Ba−Cu−O tape IEEE Trans. Appl. Supercond 13 1726–30

[116]. Trillaud F, Palanki H, Trociewitz UP, Thompson SH, Weijers HW and Schwartz J 2003 Normal zone propagation experiments on HTS composite conductors Cryogenics 43 271–9

[117]. Wang X, Trociewitz UP and Schwartz J 2007 Near-adiabatic quench experiments on short YBa2Cu3O7-delta coated conductors J. Appl. Phys 101 053904

[118]. Song H and Schwartz J 2009 Stability and quench behavior of $YBa_2Cu_3O_{7-x}$ coated conductor at 4.2 K, Self-Field IEEE Trans. Appl. Supercond 19 3735–43

[119]. Badel A, Antognazza L, Therasse M, Abplanalp M, Schacherer C and Decroux M 2012 Hybrid model of quench propagation in coated conductors for fault current limiters Supercond. Sci. Technol 25 095015

[120]. Chan WK and Schwartz J 2011 Three-dimensional micrometer-scale modeling of quenching in high-aspectratio YBa2Cu3O7-delta coated conductor tapes-part II: influence of geometric and material properties and implications for conductor engineering and magnet design IEEE Trans. Appl. Supercond 21 3628–34

[121]. Levin GA, Jones WA, Novak KA and Barnes PN 2011 The effects of superconductor–stabilizer interfacial resistance on quenching of a pancake coil made out of coated conductor Supercond. Sci. Technol 24 035015

[122]. Lacroix C, Fournier-Lupien JH, McMeekin K and Sirois F 2013 Normal zone propagation velocity in 2G HTS coated conductor with high interfacial resistance IEEE Trans. Appl. Supercond 23 4701605

[123]. Sumption MD, Majoros M, Susner M, Lyons D, Peng X, Clark CF, Lawless WN and Collings EW 2010 Thermal diffusion and quench propagation in YBCO pancake coils wound with ZnO and mylar insulations Supercond. Sci. Technol 23 075004

[124]. Ishmael S. et al. 2013; Enhanced quench propagation in $Bi_2Sr_2CaCu_2O_x$ and $YBa_2Cu_3O_{7-x}$ coils via a nanoscale doped-titania-based thermally conducting electrical insulator. IEEE Trans. Appl. Supercond. 23:7201311.

[125]. Turenne M, Johnson R, Hunte F, Schwartz J and Song H 2009 Multi-purpose fiber optic sensors for high temperature superconducting magnets 23rd IEEE/NPSS Symp. on Fusion Engineering 2009) SOFE 2009 pp 1–4

[126]. Marchevsky M, Xie YY and Selvamanickam V 2010 Quench detection method for 2G HTS wire Supercond. Sci. Technol 23 034016

[127]. Yoneda M, Nanato N, Aoki D, Kato T and Murase S 2011 Quench detection/protection of an HTS coil by AE signals Physica C: Supercond 471 1432–5

[128]. Trillaud F, Ang I, Kim W-S, Lee HG, Iwasa Y and Voccio JP 2007 Protection and quench detection of YBCO coils results with small test coil assemblies IEEE Trans. Appl. Supercond 17 2450–3

[129]. Brechna H and Turowski P 1978 Training and degradation phenomena in superconducting magnets Proc. 6th Int. Conf. on Magnet Tech. (MT-6) p 597

[130]. Tsukamoto O, Maguire JF, Bobrov ES and Iwasa Y 1981 Identification of quench origins in a superconductor with acoustic-emission and voltage measurements Appl. Phys. Lett 39 172–4

[131]. Ninomiya A, Arai K, Takano K, Ishigohka T, Kaiho K, Nakajima H, Tsuji H, Okuno K, Martovetsky N and Rodin I 2003 Diagnosis of ITER's large scale superconducting coils using acoustic emission techniques IEEE Trans. Appl. Supercond 13 1408–11

[132]. Lee H, Kim HM, Jankowski J and Iwasa Y 2004 Detection of 'hot spots' in HTS coils and test samples with acoustic emission signals IEEE Trans. Appl. Supercond 14 1298–301

[133]. Ishiyama A, Ueda H, Ando T, Naka H, Bamba S and Shiohara Y 2007 A criterion for determining stabilizer thickness of ybco coated conductors based on coil protection IEEE Trans. Appl. Supercond 17 2430–3

[134]. Uglietti D and Marinucci C 2012 Design of a quench protection system for a coated conductor insert coil IEEE Trans. Appl. Supercond 22 4702704

[135]. Dixon IR, Markiewicz WD, Murphy P, Painter TA and Powell A 2004 Quench detection and protection of the wide bore 900 MHz NMR magnet at the national high magnetic field laboratory IEEE Trans. Appl. Supercond 14 1260–3

[136]. Trociewitz UP. et al. 2008; Quench studies on a layer-wound $Bi_2Sr_2CaCu_2O_x$/AgX coil at 4.2 K. Supercond. Sci. Technol. 21:025015.

[137]. Markiewicz WD 2008 Protection of HTS coils in the limit of zero quench propagation velocity IEEE Trans. Appl. Supercond 18 1333–6

[138]. Noyes PD, Markiewicz WD, Voran AJ, Sheppard WR, Pickard KW, Jarvis JB, Weijers HW and Gavrilin AV 2012 Protection heater development for REBCO Coils IEEE Trans. Appl. Supercond 22 4704204

[139]. Gömöry F 1986 Small superconducting solenoid wound from non-insulated unstabilized multifilamentary Nb_3Sn conductor Proc. IIR Conf., Recent achievements in cryoengineering Cryoprague 86 197–202

[140]. Barkov LM, Bashtovoy NS, Bragin AV, Karpov SV, Okhapkin VS, Pivovarov SG, Ruban AA, Smakhtin VP and Snopkov IG 1999 Superconducting magnet system of the CMD-2 detector IEEE Trans. Appl. Supercond 9 4644–7

[141]. Bragin AV, Barkov LM, Karpov SV, Okhapkin VS, Popov YS, Ruban AA and Smakhtin VP 2008 Test results of the thin superconducting solenoid for the CMD-3 detector IEEE Trans. Appl. Supercond 18 399–402

[142]. Hahn S, Park D, Bascunan J and Iwasa Y 2011 HTS pancake coils without turn-to-turn insulation IEEE Trans. Appl. Supercond 21 1592–5

[143]. Kim SB, Saitou A, Joo JH and Kadota T 2011 The normalzone propagation properties of the non-insulated HTS coil in cryocooled operation Physica C: Supercond 471 1428–31

[144]. Hahn S, Park D, Voccio J, Bascunan J and Iwasa Y 2012 Noinsulation (NI) HTS inserts for >1 GHz LTS/HTS NMR magnets IEEE Trans. Appl. Supercond 22 4302405 [PubMed: 31080326]

[145]. Hahn S, Kim Y, Ling J, Voccio J, Park D, Bascunan J, Shin H-J, Lee H and Iwasa Y 2013 No-insulation coil under time-varying condition: magnetic coupling with external coil IEEE Trans. Appl. Supercond 23 4601705

[146]. Uglietti D 2013 Development of coated conductor coils without electrical insulation ICEC 24 - ICMC 2012 Proc. pp 513–6

[147]. Kim Y, Hahn S, Ling J, Kim KL, Song J, Voccio J, Bascunan J and Iwasa Y 2014 Partial-insulation winding technique for NbTi coils IEEE Trans. Appl. Supercond 24 4700505

[148]. Amemiya N and Akachi K 2008 Magnetic field generated by shielding current in high T_c superconducting coils for NMR magnets Supercond. Sci. Technol 21 095001

[149]. Decell RF 1963 Accurate low magnetic field measurements on superconducting coils Rev. Sci. Instrum 34 914–7

[150]. Mains EF. 1968; High-homogeneity tape-wound superconducting coil. J. Appl. Phys. 39:2622.

[151]. Richards DB, Edwards LR, Cornforth CM and Legvold S 1970 Vibrating sample magnetic image effects in an Nb_3Sn solenoid Rev. Sci. Instrum 41 647–9

[152]. Gu C, Qu T and Han Z 2007 Measurement and calculation of residual magnetic field in a Bi2223/Ag magnet IEEE Trans. Appl. Supercond 17 2394–7

[153]. Hahn S, Bascunan J, Kim W-S, Bobrov E, Lee H and Iwasa Y 2008 Field mapping, nmr lineshape, and screening currents induced field analyses for homogeneity improvement in LTS/HTS NMR magnets IEEE Trans. Appl. Supercond 18 856–9 [PubMed: 31889773]

[154]. Hahn S, Bascunan J, Lee H, Bobrov E, Kim W, Ahn M and Iwasa Y 2009 Operation and performance analyses of 350 and 700 MHz low-/high-temperature superconductor nuclear magnetic resonance magnets: a march toward operating frequencies above 1 GHz J. Appl. Phys 105 024501

[155]. Ahn M, Yagai T, Hahn S, Ando R, Bascunan J and Iwasa Y 2009 Spatial and temporal variations of a screening current induced magnetic field in a double-pancake HTS Insert of an LTS/HTS NMR magnet IEEE Trans. Appl. Supercond 19 2269–72 [PubMed: 20401187]

[156]. Yanagisawa Y, Nakagome H, Uglietti D, Kiyoshi T, Hu R, Takematsu T, Takao T, Takahashi M and Maeda H 2010 Effect of YBCO-coil shape on the screening current-induced magnetic field intensity IEEE Trans. Appl. Supercond 20 744–7

[157]. Yanagisawa Y, Kominato Y, Nakagome H, Hu R, Takematsu T, Takao T, Uglietti D, Kiyoshi T, Takahashi M and Maeda H 2011 Magnitude of the screening field for YBCO coils IEEE Trans. Appl. Supercond 21 1640–3

[158]. Otsuka A, Yanagisawa Y, Kiyoshi T, Maeda H, Nakagome H and Takeda M 2011 Evaluation of the screening current in a 1.3 GHz NMR magnet using ReBCO IEEE Trans. Appl. Supercond 21 2076–9

[159]. Uglietti D, Yanagisawa Y, Maeda H and Kiyoshi T 2010 Measurements of magnetic field induced by screening currents in YBCO solenoid coils Supercond. Sci. Technol 23 115002

[160]. Iwasa Y, Hahn S, Voccio J, Park DK, Kim Y and Bascunan J 2013 Persistent-mode high-temperature superconductor shim coils: a design concept and experimental results of a prototype Z1 high-temperature superconductor shim Appl. Phys. Lett 103 52607 [PubMed: 23983275]

[161]. Yanagisawa Y, Nakagome H, Koyama Y, Hu R, Takao T, Hamada M, Kiyoshi T, Takahashi M and Maeda H 2009 Effect of current sweep reversal on the magnetic field stability for a Bi-2223 superconducting solenoid Physica C: Supercond 469 1996–9

[162]. Kajikawa K and Funaki K 2011 A simple method to eliminate shielding currents for magnetization perpendicular to superconducting tapes wound into coils Supercond. Sci. Technol 24 125005

[163]. National Research Council 2013 High Magnetic Field Science and Its Application in the United States: Current Status and Future Directions (Washington, DC: National Academies Press)

[164]. Bascunan J, Hahn Y, Kim Y and Iwasa Y 2013 An 18.8 T/90 mm bore all-HTS insert (H800) for 1.3 GHz LTS/HTS NMR magnet: insert design and double pancake coil fabrication IEEE Trans. Appl. Supercond 24 4300904

[165]. Bascunan J, Hahn S, Park D, Kim Y and Iwasa Y 2012 On the 600 MHz HTS insert for a 1.3 GHz NMR magnet IEEE Trans. Appl. Supercond 22 4302104 [PubMed: 31171896]

[166]. Bascunan J, Hahn S, Kim Y and Iwasa Y 2013 A new hightemperature superconducting (HTS) 700 MHz insert magnet for a 1.3 GHz LTS/HTS NMR magnet IEEE Trans. Appl. Supercond 23 4400304

[167]. Otsuka A, Kiyoshi T and Takeda M 2010 A 1.3 GHz NMR magnet design under high hoop stress condition IEEE Trans. Appl. Supercond 20 596–9

[168]. Kiyoshi T et al. 2010 HTS-NMR: present status and future plan IEEE Trans. Appl. Supercond 20 714–7

[169]. Matsumoto S, Kiyoshi T, Otsuka A, Hamada M, Maeda H, Yanagisawa Y, Nakagome H and Suematsu H 2012 Generation of 24 T at 4.2 K using a layer-wound GdBCO insert coil with Nb3Sn and Nb–Ti external magnetic field coils Supercond. Sci. Technol 25 025017

[170]. www.magnet.fsu.edu/usershub/publications/sciencehighlights/

[171]. Weijers HW. et al. 2014; Progress in the development of a superconducting 32 T magnet with REBCO high field coils. IEEE Trans. Appl. Supercond. 24:4301805.

[172]. Awaji S, Ishihara R, Namba M, Nishijima G, Oguro H, Watanabe K, Shikimachi K, Hirano N and Nagaya S 2010 Upgrading design to a 25 T cryogen-free superconducting magnet based on low temperature and high magnetic field properties of the practical CVD processed coated conductors IEEE Trans. Appl. Supercond 20 592–5

[173]. Awaji S. et al. 2014; New 25 T cryogen-free superconducting magnet project at tohoku university. IEEE Trans. Appl. Supercond. 24:4302005.

[174]. Koyanagi K, Ono M, Hanai S, Watanabe K, Awaji S, Hamajima T, Kiyoshi T and Kumakura H 2009 Design of a 30 T superconducting magnet using a coated conductor insert IEEE Trans. Appl. Supercond 19 1617–20

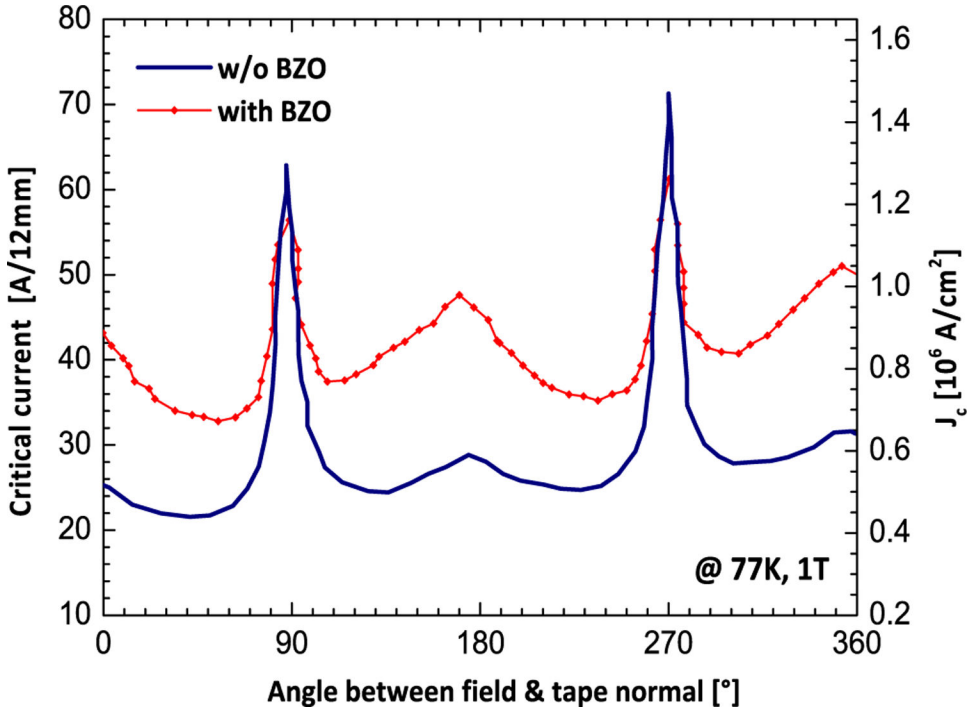

Figure 1.

Effects of BZO inclusions on the angular dependence of the critical current, at T=77 K and B=1 T. Data extracted from [40].

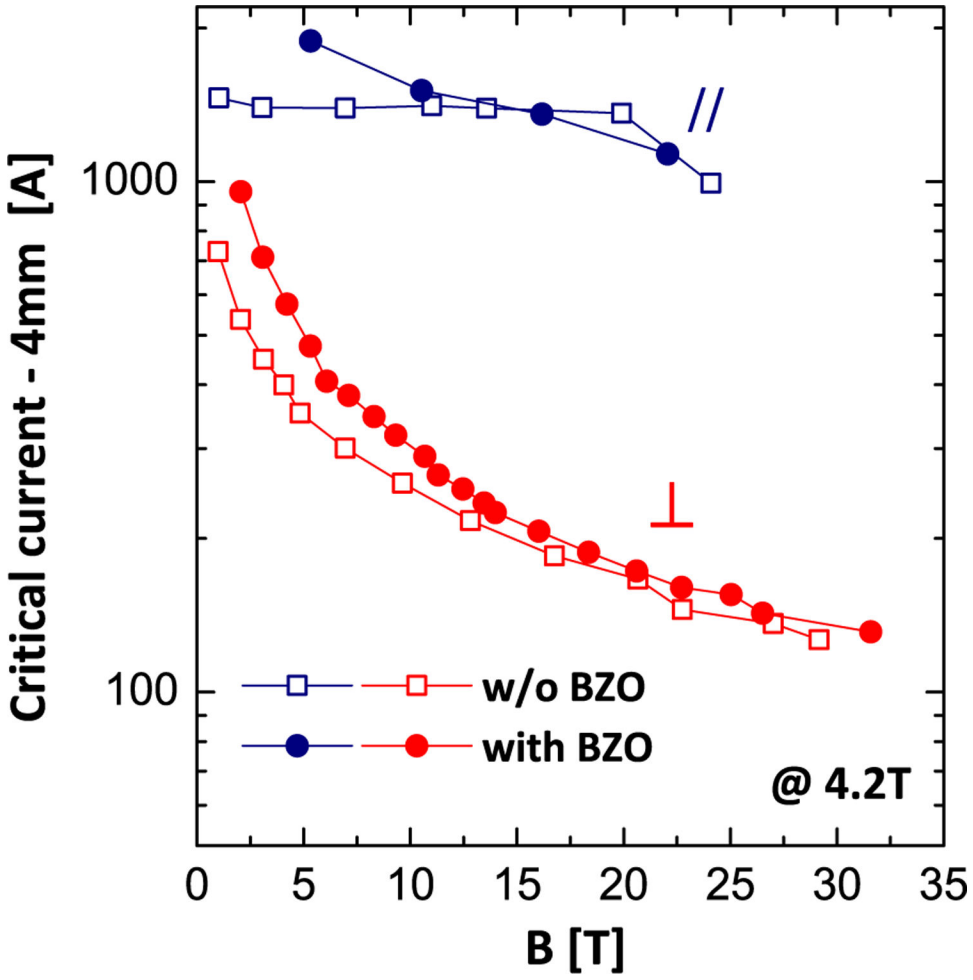

Figure 2.
4.2 K Critical current $I_c(B)$ plots for coated conductors with and without BZO. The field is oriented parallel (blue) and perpendicularly (red) to the tape surface. Data extracted from [41].

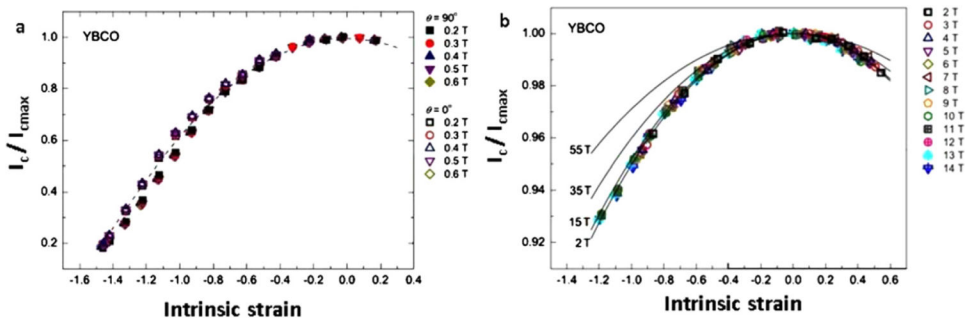

Figure 3.

(a) Normalized 77 K critical current versus intrinsic strain plots of an Y123 coated conductor for selected fields applied parallel and perpendicular to the *c*-axis. (b) Normalized 4.2 K critical current versus intrinsic strain plots in selected magnetic fields in the range 2–14 T parallel to the *c*-axis. Reprinted from [52].

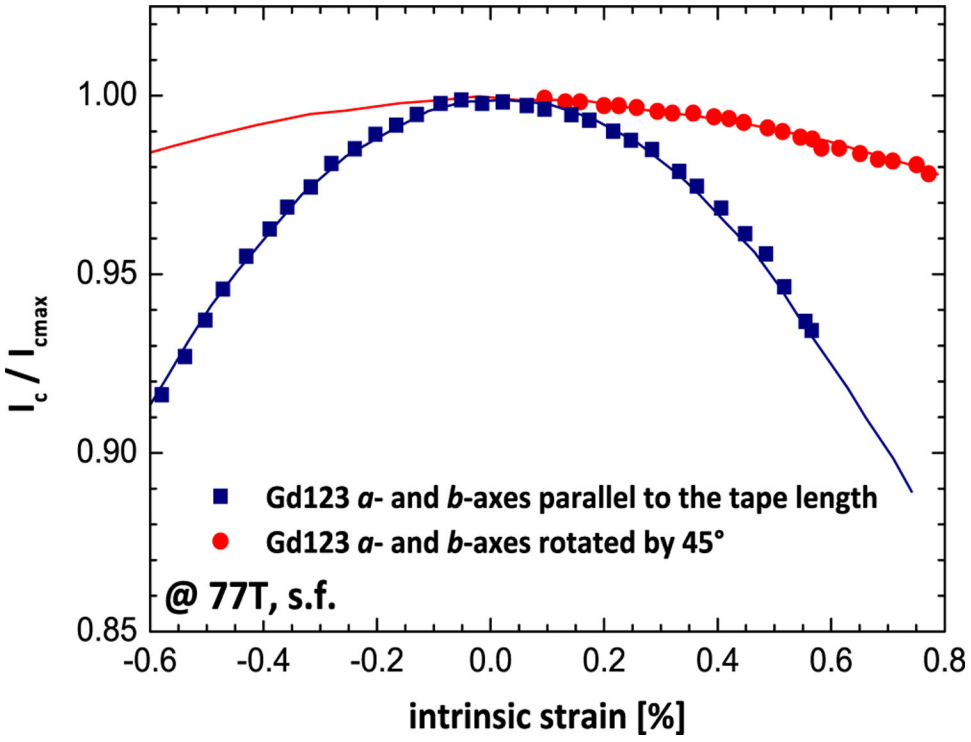

Figure 4.

77 K I_c versus strain plots: blue squares correspond to *a* and *b*-axis of the Gd123 film oriented parallel to the tape length, red circles correspond to *a* and *b*-axis of the Gd123 film rotated by 45° from the longitudinal direction [56].

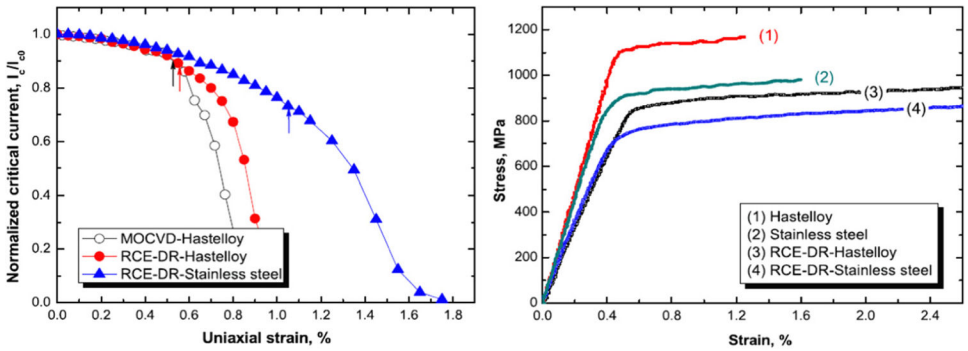

Figure 5.

Normalized 77 K I_c versus strain curves for coated conductors with different substrates in self field (left graph). Stress-strain curves for substrate materials and Cu-stabilized coated conductor tapes. Reprinted from [65].

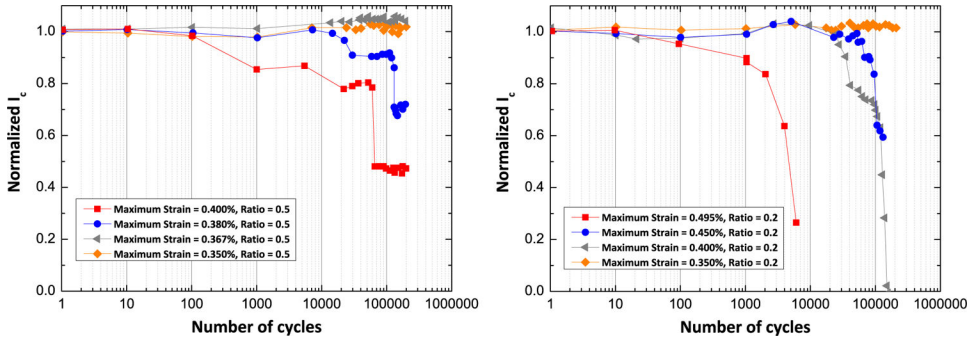

Figure 6.

$I_c(N)/I_c(N=0)$ versus the number of cycles N for samples subjected to fatigue test with a strain ratio of 0.5 (left) and 0.2 (right). Dataextracted from [69].

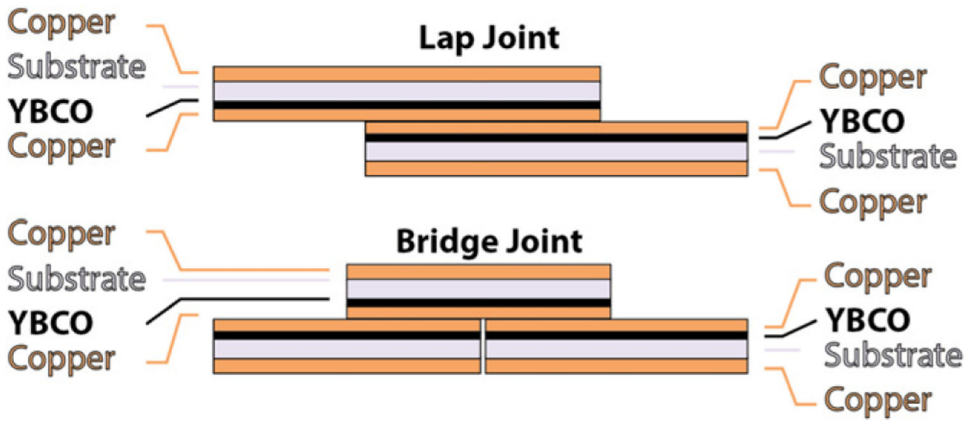

Figure 7.
Different joint configurations: lap joint (top) and bridge joint (bottom).

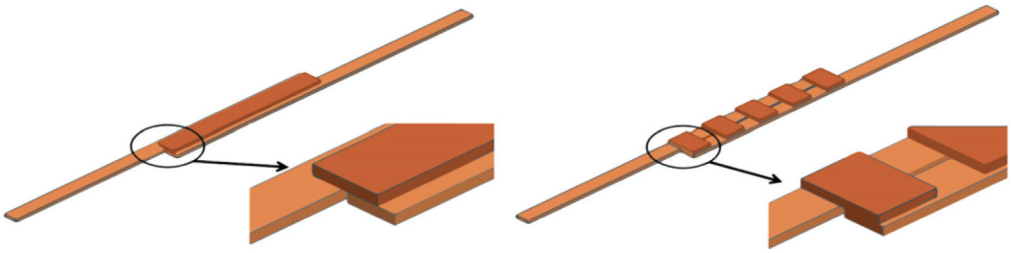

Figure 8.
Different configuration of bridge joints. Left: PD joint; right: OD joint.

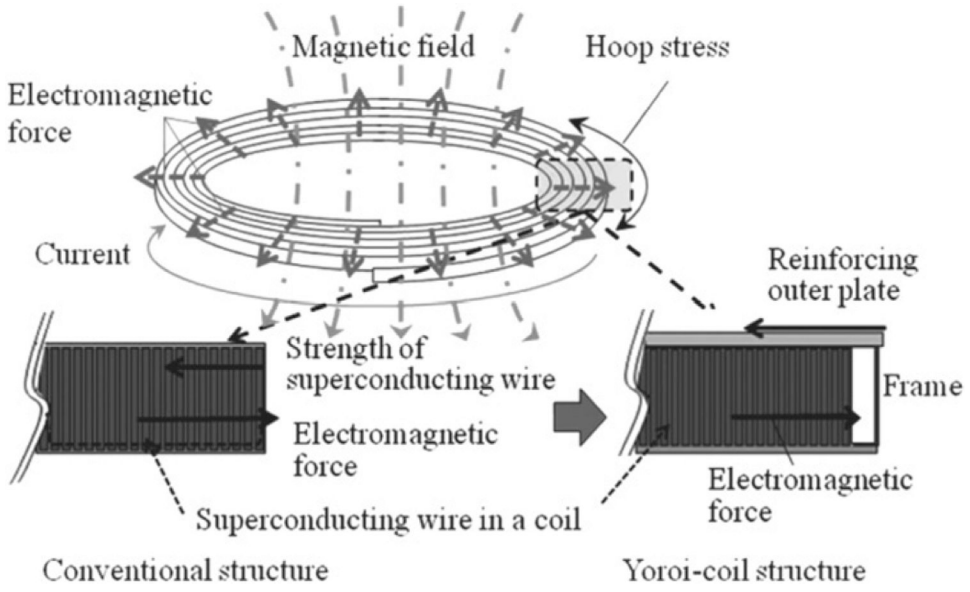

Figure 9.

Schematic of supporting mechanism of 'Yoroi-coil' structure against electromagnetic force. Reprinted with permission from Nagaya *et al IEEE Trans. Appl. Supercond.* **23** 4601204 [113], copyright 2013, IEEE.

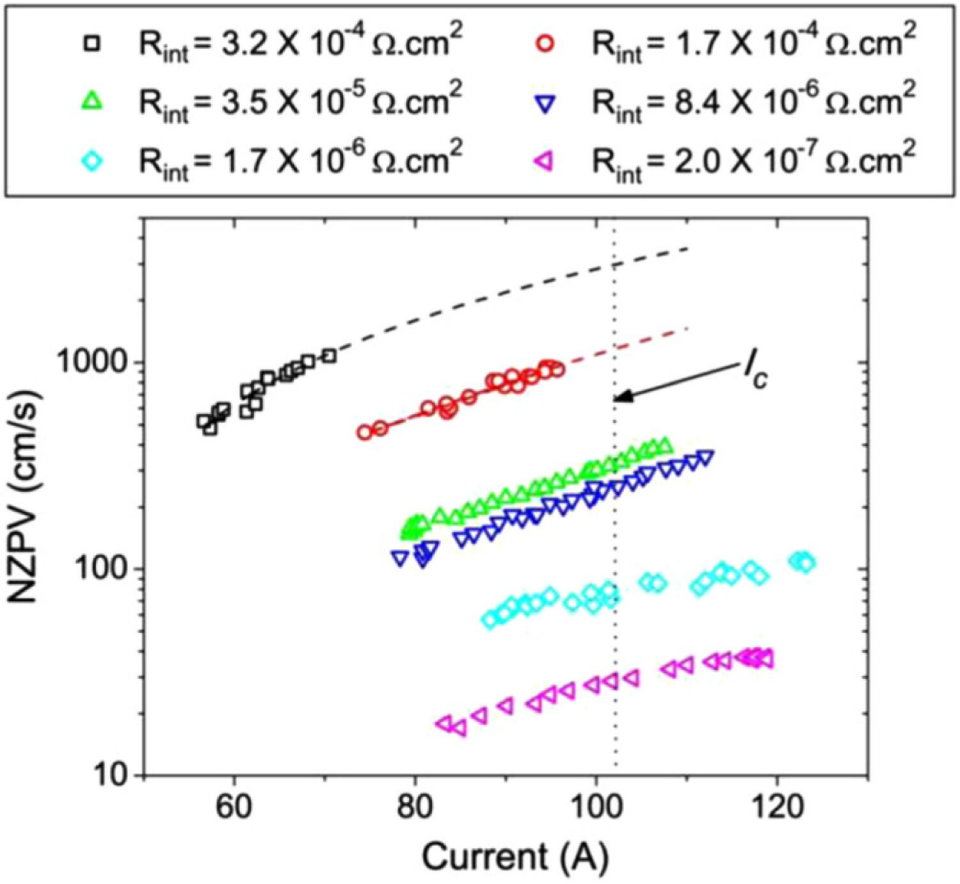

Figure 10.

Dependence of NZPV with applied current at 77 K in self-field, for different values of the interfacial resistance between the ceramic layer and the stabilizer. Reprinted with permission from Lacroix *et al IEEE Trans. Appl. Supercond.* **23** 4701605 [122], copyright 2013, IEEE.

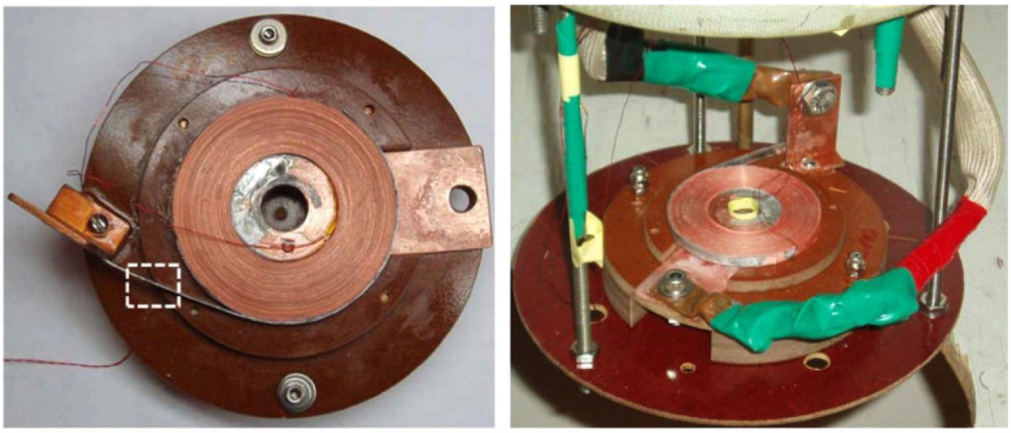

Figure 11.

(a) No-Insulation (NI) HTS single pancake test coil; (b) test coil mounted in the LHe experimental setup. Reprinted with permission from Hahn *et al IEEE Trans. Appl. Supercond.* **22** 4302405 [144], copyright 2012, IEEE.

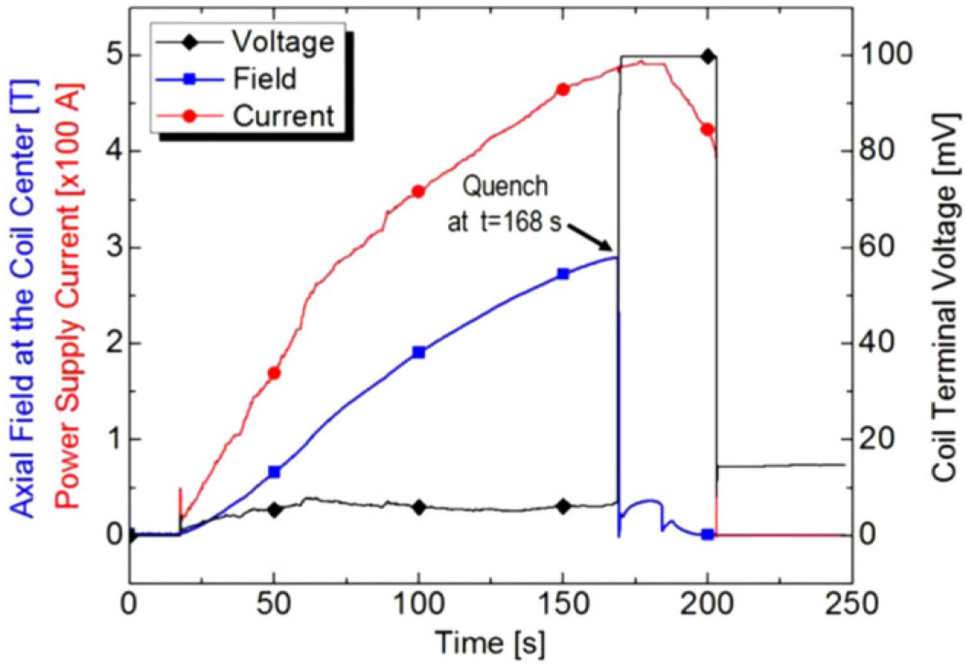

Figure 12.

Over-current test results of an NI HTS test coil at 4.2 K. Reprinted with permission from Hahn *et al* IEEE *Trans. Appl. Supercond.* **22** 4302405 [144], copyright 2012, IEEE.

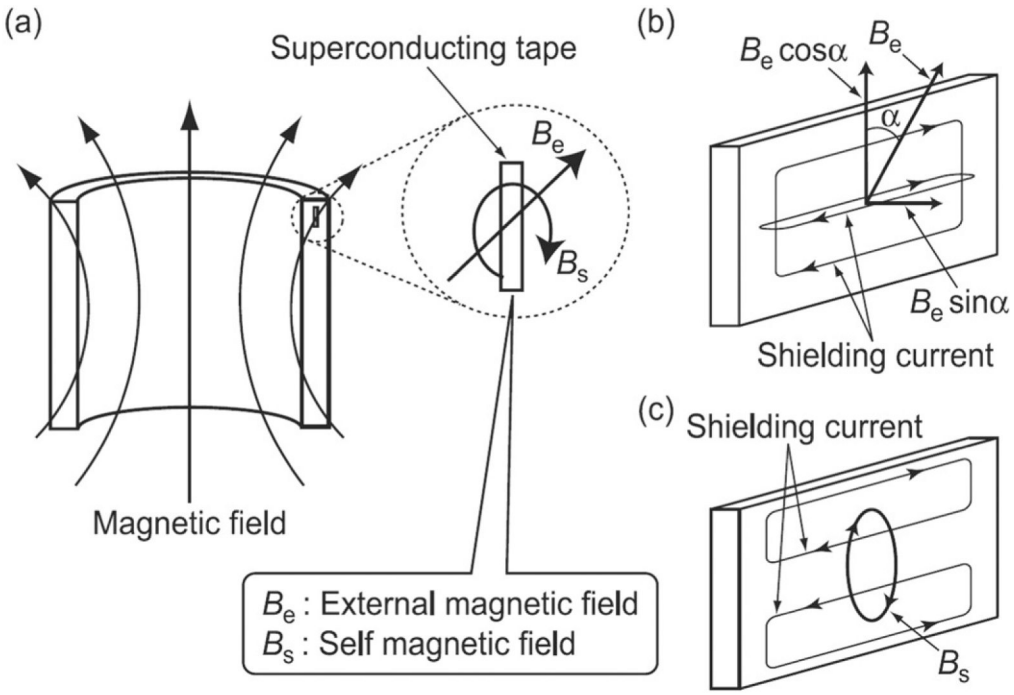

Figure 13.

Magnetic fields and shielding currents in superconducting tape: (a) external magnetic field B_e and self-magnetic field B_s for superconducting tape, (b) shielding (magnetization) current against B_e, and (c) shielding current against B_s. Reprinted from [148].

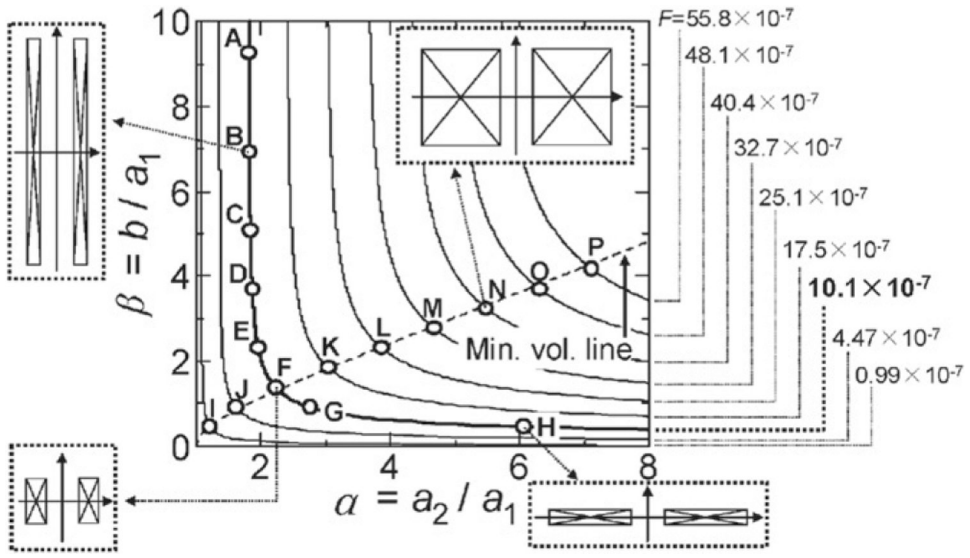

Figure 14.

Lines of constant shape factor F as a function of the coil geometry: $2a_1$ is the bore diameter, $2a_2$ the coil diameter and $2b$ the coil height. Coils on the same line generate the same central magnetic field, if the overall current density and the inner diameter are the same. Coils on the minimum volume line generate a central magnetic field with minimum use of superconducting wire. Reprinted with permission from Yanagisawa *et al IEEE Trans. Appl. Supercond.* **20** 744–7 [156], copyright 2011, IEEE.

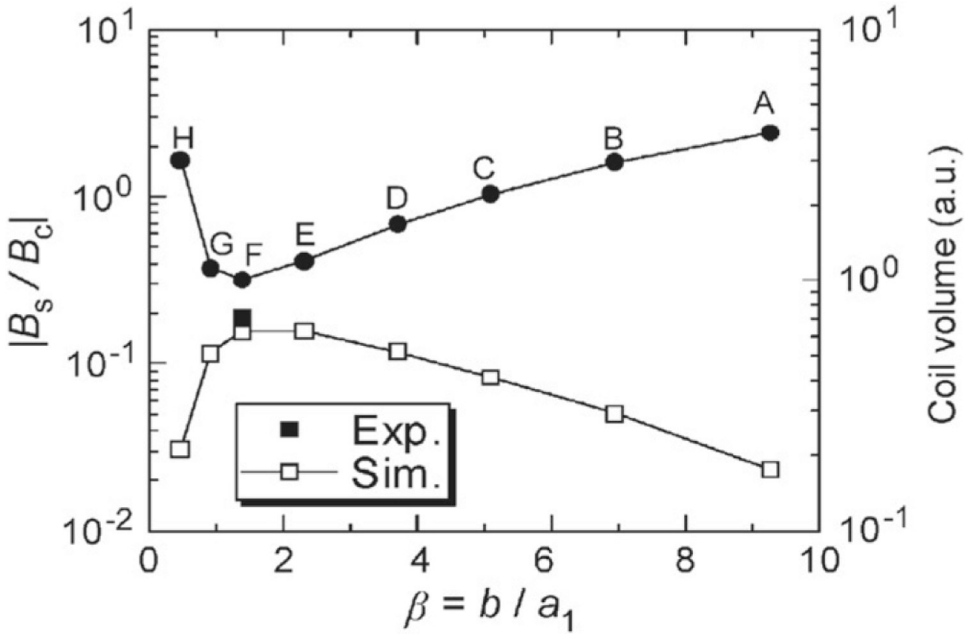

Figure 15.

The ratio between the screening field and the design central field as a function of the coil height normalized to the bore diameter. Reprinted with permission from Yanagisawa *et al IEEE Trans. Appl.* Supercond. **20** 744–7 [156], copyright 2011, IEEE.

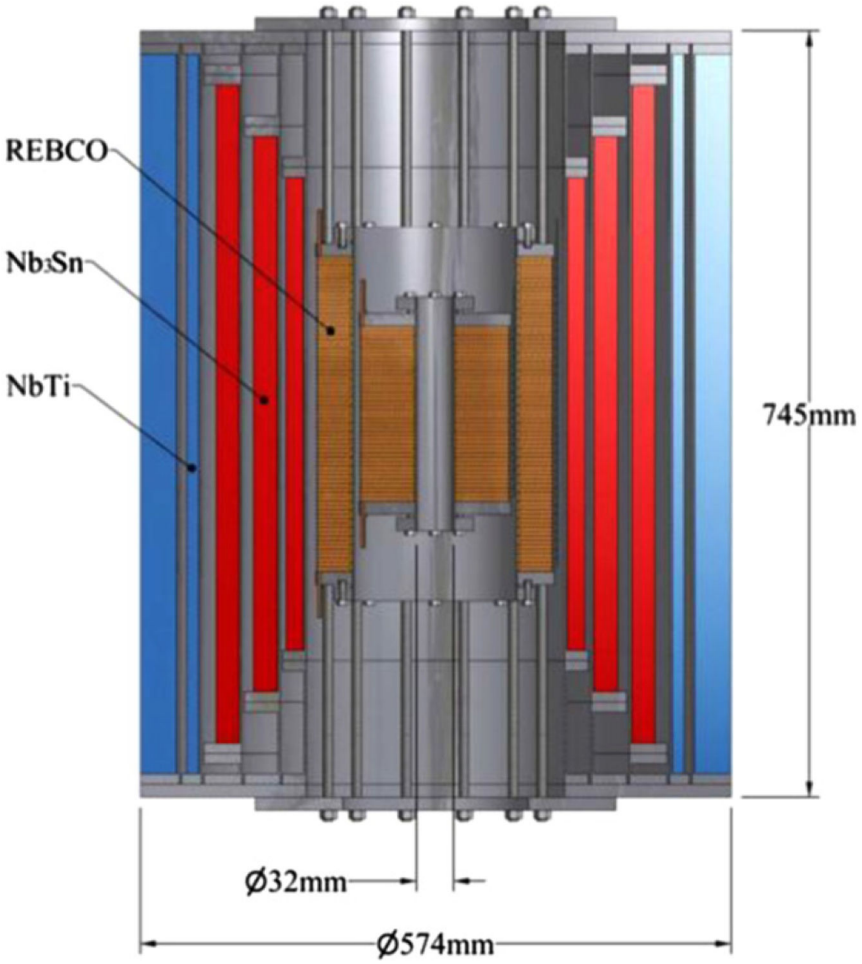

Figure 16.
Design of a superconducting 32 T magnet with RE123 high field coils, from NHMFL. Reprinted from [170].

Table 1.

Fabrication process and template of industrial coated conductors

Manufacturer	Technique	Substrate	Buffer layers	HTS
AMSC	RABiTS/MOD	NiW	Y_2O_3/YSZ/CeO_2	Y123
SuperPower	IBAD/MOCVD	Hastelloy	Al_2O_3/Y_2O_3/MgO/$LaMnO_3$	Gd123
Bruker[a]	ABAD/PLD	Stainless steel	YSZ/CeO_2	Y123
Fujikura	IBAD/PLD	Hastelloy	Al_2O_3/Y_2O_3/MgO/CeO_2	Gd123
SuperOx	IBAD/PLD	Hastelloy	Al_2O_3/Y_2O_3/MgO/$LaMnO_3$/CeO_2	Gd123
Sumitomo[a]	RABiTS/PLD	NiW	CeO_2/YSZ/CeO_2	Gd123
SuNAM	IBAD/RCE	Hastelloy or stainless steel	Al_2O_3/Y_2O_3/MgO/$LaMnO_3$	Gd123
STI[a]	IBAD/RCE	Hastelloy	Y_2O_3-Al_2O_3/MgO	Y123

[a]As yet marketplace conductor.

Table 2.

Substrate materials, electrical and mechanical stabilization of industrial coated conductors.

	AMSC	Fujikura	SuNAM	SuperPower
Substrate	75 μm NiW	75–100 μm Hastelloy C276	60 μm Hastelloy C276 or >80 μm stainless steel	50–100 μm Hastelloy C276
Lamination	50 μm copper or 150 μm brass or 25–75 μm stainless steel	75–100 μm one side	brass available	na
Electroplated copper	na	na	15 μm both sides	20–50 μm both sides

Table 3.

Stress limits for a coated conductor under various mechanical constraints [73].

Type of stress	Stress (Mpa)	Scheme
Axial (50 μm thick Hastelloy substrate)	>700	
Transverse	~10–100	
Transverse compressive	>100	
Shear stress	>19	
Cleavage	<1	
Peel		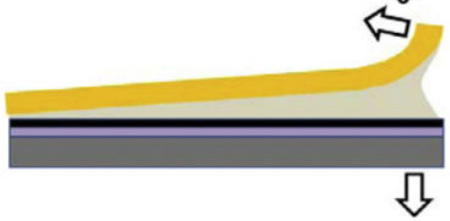

Table 4.

Main parameters of the ongoing high-field projects based on RE123.

	35.4 T NHMFL	1.3 GHz MIT	32 T NHMFL	24 T NIMS	25 T CSM HFLSM	100 T MIT
Target field *(T)*	35.4	30.5	32	24	25.6	100
RE123 coil field (*T*)	4.2	18.8	17	7.6	11.5	100
No. RE123 sections	1	3	2	1	1	39
Inner diameter (mm)	14	91	40	50	96	20
Outer diameter (mm)	38	204	232	112.4	280	5600
Winding technology	LW	DP	DP	LW	LW	DP
Operating current	196	250	180	360	135	4 × 600
Winding curr. dens. (A mm^{-2})	320	546	197/176	262	110.8	520.8
Copper curr. dens.(A mm^{-2})	1200	2042*	439	960	—	—
Max. Hoop stress (MPa)	340	680	450	450	405	398
Total RE123 (m)	96	11’590	9’379	515	17’591	12’367’000
Status	Tested	In prod.	In prod.	Tested	Concept	Concept